Leptin Activated Hypothalamic BNC2 Neurons Acutely Suppress Food Intake

Han L. Tan[1], Luping Yin[2], Yuqi Tan[3], Jessica Ivanov[1], Kaja Plucinska[4], Anoj Ilanges[1], Brian R. Herb[5], Putianqi Wang[1], Christin Kosse[1], Paul Cohen[4], Dayu Lin[2], Jeffrey M. Friedman[1*]

[1] Laboratory of Molecular Genetics, Howard Hughes Medical Institute, The Rockefeller University, New York, NY, USA

[2] Department of Psychiatry, Neuroscience Institute, New York University Langone Medical Center, New York, NY, USA

[3] Department of Microbiology and Immunology, Stanford University School of Medicine, Stanford, CA, USA

[4] Laboratory of Molecular Metabolism, The Rockefeller University, New York, NY, USA

[5] Institute for Genome Sciences, Department of Pharmacology, University of Maryland School of Medicine, Baltimore, MD, USA

* Corresponding author: JMF, friedj@rockefeller.edu

Abstract:

Leptin is an adipose tissue hormone that maintains homeostatic control of adipose tissue mass by regulating the activity of specific neural populations controlling appetite and metabolism[1]. Leptin regulates food intake by inhibiting orexigenic agouti-related protein (AGRP) neurons and activating anorexigenic pro-opiomelanocortin (POMC) neurons[2]. However, while AGRP neurons regulate food intake on a rapid time scale, acute activation of POMC neurons has only a minimal effect[3-5]. This has raised the possibility that there is a heretofore unidentified leptin-regulated neural population that suppresses appetite on a rapid time scale. Here, we report the discovery of a novel population of leptin-target neurons expressing basonuclin 2 (*Bnc2*) that acutely suppress appetite by directly inhibiting AGRP neurons. Opposite to the effect of AGRP activation, BNC2 neuronal activation elicited a place preference indicative of positive valence in hungry but not fed mice. The activity of BNC2 neurons is finely tuned by leptin, sensory food cues, and nutritional status. Finally, deleting leptin receptors in BNC2 neurons caused marked hyperphagia and obesity, similar to that observed in a leptin receptor knockout in AGRP neurons. These data indicate that BNC2-expressing neurons are a key component of the neural circuit that maintains energy balance, thus filling an important gap in our understanding of the regulation of food intake and leptin action.

Main:

Leptin is an adipose tissue-derived hormone that functions as the afferent signal in a negative feedback loop that maintains homeostatic control of adipose tissue mass[1,6]. Leptin regulates food intake and maintains energy balance in part by inhibiting orexigenic agouti-related protein (AGRP)/neuropeptide Y (NPY) neurons, expressing leptin receptor (LepR), and activating anorexigenic pro-opiomelanocortin (POMC) neurons, also expressing LepR[1,2]. These neurons are located in the arcuate nucleus (ARC) of the hypothalamus, adjacent to the median eminence, the site of a circumventricular organ that has fenestrated capillaries enabling signaling without transit across the blood-brain barrier. POMC is a protein precursor that is proteolytically cleaved to generate alpha-melanocyte stimulating hormone (aMSH) which reduces food intake by activating the melanocortin 4 receptor (MC4R) which is widely distributed throughout the brain[7,8]. AGRP/NPY neurons increase food intake via projections to many of the same sites as POMC neurons where the AGRP protein diminishes aMSH signaling at the MC4 receptor[7,8]. AGRP/NPY neurons also directly inhibit POMC neurons[9]. These findings have suggested that food intake is reciprocally regulated by these two neural populations. This proposed 'yin-yang' dynamic between these neural populations is a consistent feature in nearly all models of how the homeostatic control of food intake and body weight is maintained[10]. However, while leptin acutely reduces food intake, particularly in ob/ob mice, this response cannot be fully accounted for by modulation of AGRP/NPY or POMC neurons[11,12]. Moreover, the functional effects and dynamics of POMC and AGRP/NPY neurons diverge in several important respects and several lines of evidence have suggested that there may be additional leptin-responsive populations that are crucial for leptin-driven control of food intake and body weight[13,14].

First, while activating AGRP/NPY neurons rapidly leads to food seeking and consumption, activating POMC neurons has only a minimal effect to acutely reduce food intake[3-5]. Second, mutations in POMC, POMC processing enzymes, or the MC4R cause obesity[7,8,15], whereas mutations in AGRP and NPY have not been reported to alter body weight although ablation of these neurons has been reported to cause anorexia[16-20]. In addition, while activation of AGRP/NPY neurons is associated with negative valence, POMC neuron activation is not associated with positive valence but rather also elicits negative valence[21,22]. The role of these populations in leptin signaling has also been evaluated and while a knockout of the LepR in AGRP/NPY neurons of adult mice causes extreme obesity, deletion of the LepR from adult POMC neurons has only a minimal effect[23]. Finally, acute activation of AGRP/NPY neurons alters glucose metabolism, a response not observed with acute manipulation of POMC neurons[24]. Thus, while POMC and AGRP/NPY neurons have opposite effects on weight, their effects are not equivalent

in other respects, indicating that they are not precise counterparts. This has raised the possibility that there might be a missing population of LepR-expressing neurons that acutely suppresses food intake with a time course similar to the effects of AGRP/NPY neurons.

To address this, we conducted a systematic profiling of the transcriptomes of ARC neurons using single nucleus RNA sequencing (snRNA-seq) and identified a novel population of LepR-expressing ARC neurons that co-express the basonuclin 2 (*Bnc2*) gene. Further studies revealed that BNC2 neurons rapidly induce satiety with similar kinetics to the activation of feeding after AGRP/NPY neural activation. This discovery adds an important new cellular component to the neural network that regulates hunger and satiety and sheds new light on how leptin regulates energy balance.

Results

Identification of novel LepR-expressing neurons in the ARC

We performed snRNA-seq on ARC that was micro-dissected from adult mice (**Fig.1a**). Nuclei were isolated, stained with a fluorescent antibody to NeuN, a specific marker of neuronal nuclei, and subjected to fluorescent activated sorting followed by single nucleus sequencing using the 10X single-cell analysis platform[25]. A total of 3,557 cells were profiled, of which 3,481 were identified as neurons based on the expression levels of neuronal markers including *Tubb3*, *Snap25*, *Syt1*, and *Elavl4,* and the absence of non-neuronal markers (**Extended Data Fig. 1a,b**). Leiden clustering analysis identified 21 distinct neuron clusters (**Fig. 1b,c**). To confirm that these neurons were from the ARC rather than from adjacent regions, we analyzed the clusters for specific marker genes that define known ARC populations. This validation process confirmed that 19 of the clusters were indeed located within the ARC with the exception of clusters 9 and 15, which express *Nr5a1*, indicating their origin from the adjacent ventromedial hypothalamus (VMH) region (**Fig. 1c**)[26,27]. These clusters included one AGRP/NPY (Cluster 0), two POMC-expressing (Clusters 3 and 12) neurons, and 16 additional clusters (**Fig. 1d**). Clusters 0 and 3 expressed the LepR as did Cluster 17 which did not express AGRP, NPY, or POMC but instead was characterized by the expression of the *Bnc2* gene (**Fig. 1d**). Several of the genes in BNC2 Cluster 17 including *Lepr* were also found in a single cluster (n11.Trh/Cxcl12) in a previously published dataset of ARC neuron types[26] (**Extended Data Fig. 1c**). However, *Bnc2* was not identified in this cluster and thyrotropinreleasing hormone (*Trh)*, the canonical marker, was also expressed in other clusters that did not express LepR[26]. Thus, BNC2 serves as a specific marker for a novel LepR cluster that does not include AGRP, NPY or POMC.

102 The total number of cells in the BNC2 cluster (Cluster 17, n=35) was lower than those in
103 the AGRP cluster (Clusters 0, n=650) or the POMC cluster (Cluster 3, n=271). However, the level
104 of LepR expression in the cells in this cluster was significantly higher than in the POMC cluster
105 and equivalent to that in the AGRP cluster (Cluster 0: 1.32; Cluster 3: 0.52; Cluster 17: 1.09). We
106 confirmed the co-expression of LepR and BNC2 using multiplex RNA in situ hybridization of adult
107 mouse hypothalamus. The results showed that over 90% of *Bnc2* cells in the ARC co-expressed
108 *Lepr* (90.4%) and *Slc32a1* (96.6%), a marker for inhibitory GABAergic neurons while less than 5%
109 co-expressed either *Agrp* (2.6%) and *Pomc* (3.3%) (**Fig. 1e,f**). We also determined whether BNC2
110 co-localized with LepR in human hypothalamus ARC and found a significant overlap between
111 *Bnc2* and *Lepr* (Fisher's exact test, p=0.0218, **Fig. 1g**). Here again, the LepR/BNC2 cells in
112 human hypothalamus were distinct from AGRP/NPY and POMC neurons, as 82.1% (23 out of 28)
113 of LepR/BNC2 neurons were not co-localized with *Agrp*, *Npy*, or *Pomc* (**Fig. 1h**). Altogether, these
114 results show that BNC2 neurons are a novel population of LepR-expressing neurons in mouse
115 and human that are non-overlapping with the previously characterized LepR AGRP/NPY and
116 POMC populations. Spatial transcriptome data from the Allen Brain Institute confirms
117 hypothalamic expression of BNC2 with limited expression elsewhere in the brain other than in the
118 cortex and hippocampus[28].
119
120 **Activation of BNC2 neurons by leptin, refeeding, and food cues**
121 In order to further study the dynamics and function of BNC2 neurons in ARC, we generated
122 a BNC2-P2A-iCre knockin mouse line (referred to hereafter as BNC2-Cre) by inserting a P2a-
123 iCre fusion in frame at the C-terminus of the BNC2 protein[29] (**Extended Data Fig. 2a,b**). The
124 correct insertion site of iCre was confirmed using PCR of genomic DNA (**Extended Data Fig. 2c**).
125 Eutopic expression of Cre in BNC2 neurons in ARC was verified by injecting an AAV virus with a
126 Cre-dependent mCherry into the ARC of adult BNC2-Cre mice. This showed nearly complete co-
127 localization of mCherry and *Bnc2* RNA (**Extended Data Fig. 2d**). Leptin binding to LepR activates
128 Janus tyrosine kinase 2 (Jak2), leading to STAT3 phosphorylation, a canonical marker of leptin
129 activation[30] and we confirmed leptin signaling in BNC2 neurons by immunostaining for pSTAT3.
130 An AAV expressing a DIO-mCherry cassette was injected into the ARC of adult BNC2-Cre mice
131 and animals subsequently received a single injection of leptin (3 mg/kg) after an overnight fast.
132 This resulted in a significant increase in pSTAT3 in mCherry labeled BNC2 neurons at 3 hours,
133 not seen in control animals that received PBS injections (**Fig. 2a,b**). Refeeding mice after an
134 overnight fast also led to a significant increase of pSTAT3 levels in BNC2 neurons (**Fig. 2a,b**).

135 Consistent with this we also found that the levels of cFos, a neuron activity marker [31], significantly
136 increased in BNC2 neurons following refeeding or leptin injection (**Fig. 2c,d**).
137 We then performed whole-cell patch-clamp recordings in hypothalamic slices prepared
138 from adult BNC2-Cre mice injected with a DIO-EGFP AAV in the ARC. Application of leptin (100
139 nM) to brain slices prepared from either fasted or ad-libitum-fed mice resulted in a substantial
140 increase in action potential (AP) firing rates in GFP labeled BNC2 neurons (Fast: 0.01±0.0.005
141 Hz and 0.488±0.188 Hz before and after leptin, respectively, p=0.0157; Fed: 0.014±0.012 Hz and
142 0.235±0.118 Hz before and after leptin, respectively, p=0.0062) and a significant depolarization
143 (Fast: -58.02±2.24 mV and -46.41±2.69 mV before and after leptin, respectively, p < 0.0001; Fed:
144 -50.13±1.92 mV and -44.92±2.83 mV before and after leptin, respectively, p=0.0074. **Fig. 2e-g,**
145 **Extended Data Fig.3**). These effects were reversible after leptin washout (**Fig. 2e-g, Extended**
146 **Data Fig.3**). In addition, a higher percentage of cells responded to leptin in the slices prepared
147 after an overnight fast (16 out of 17) compared to those responding in slices prepared from ad-
148 libitum-fed mice (7 out of 12) (**Fig. 2h**). The greater effect of leptin on neurons from fasted
149 hypothalamus is consistent with the cFos data showing that the baseline activity of BNC2 neurons
150 is lower after an overnight fast (**Fig. 2d**).
151 To assess the in vivo responses, we employed fiber photometry to record the effect of food
152 cues on the activity of BNC2 neurons. We injected a DIO-GCamp6s AAV into the ARC of adult
153 BNC2-Cre mice and implanted a fiber above the ARC to record neural activity. Mice were fasted
154 overnight after which an inedible plastic tube, a pellet of standard chow, or peanut butter was
155 provided. The inedible tube did not have a discernible effect on BNC2 neuron activity (**Fig. 3a-c,**
156 **Extended Data Fig. 4a-c**). However, exposure to standard chow robustly activated BNC2
157 neurons within seconds relative to the plastic tube (Delta F/F: 0.08±0.13 and 2.83±0.99 for tube
158 and chow, respectively; p=0.0078, **Fig. 3a-c, Extended Data Fig. 4a-c**) and exposure to peanut
159 butter, which has a significantly higher fat content, elicited a significantly greater response than
160 did chow (Delta F/F: 4.44±1.36 for peanut butter, p=0.0078, **Fig. 3a-c, Extended Data Fig. 4a-**
161 **c**). In contrast, BNC2 neurons from ad-libitum-fed mice showed little or no response to the inedible
162 tube and standard chow (**Fig. 3d,e, Extended Data Fig. 4d-f**) while peanut butter still significantly
163 activated BNC2 neurons (Delta F/F: 0.001±0.322 and 2.764±1.093 for chow and peanut butter,
164 respectively; p=0.0078; **Fig. 3d,e, Extended Data Fig. 4d-f**). These results show that the activity
165 of BNC2 neurons is increased by the presence of food and that this is augmented by palatability
166 and sensitive to nutritional state (i.e; fed vs fasted).
167 We further noted that the increased fluorescence of BNC2 neurons preceded the initiation
168 of food intake suggesting that they were activated by sensory cues (**Fig. 3f, Supplementary**

169 **Video1**). We tested this directly by presenting mice with standard chow in a container that allowed
170 them to see and smell the pellet without being able to consume it (**Fig. 3g**). Under these conditions,
171 BNC2 neurons still showed significant activation albeit of lesser magnitude and duration
172 compared to the experiments in which the food was not caged (Delta F/F: 1.287±0.567 and
173 2.354±0.87 for caged and free, respectively; p=0.0156, **Fig. 3h,i, Extended Data 4g,h**). This
174 suggests BNC2 neurons respond to sensory cues and that accessibility to food further modulates
175 the strength and duration of neural activation. Finally, we examined whether the removal of food
176 extinguished the neural activation seen after food presentation. In this experiment, mice that had
177 been fasted overnight were presented with accessible chow which was removed 2 or 10 minutes
178 after it was provided. Removal of food led to a rapid decrease in the activity of BNC2 neurons
179 (**Fig. 3j-l, Extended Data 4i-j**). In contrast, the BNC2 neurons remained active when food was
180 continuously present. (**Fig. 3j-l, Extended Data 4i-j**).
181
182 **BNC2 neurons acutely suppress food intake**
183 We next assessed the function of BNC2 neurons using chemogenetics and optogenetics.
184 AAVs expressing a Cre-dependent stimulatory hM3Dq (Gq-coupled human muscarinic M3
185 designer receptors exclusively activated by designer drugs, DREADD) or an inhibitory hM4Di
186 DREADD were injected into the ARC of BNC2-Cre mice. Mice receiving a virus expressing
187 mCherry and given CNO, as well as mice receiving the DREADD and given PBS were used as
188 controls in these and subsequent experiments. We then selectively activated or inhibited these
189 neurons using clozapine-N-oxide (CNO)[32]. Activating BNC2 neurons at the beginning of the dark
190 cycle resulted in a significant reduction in food intake and body weight compared to control mice
191 (3h food intake: 1.1±0.11 g and 0.52±0.08 g for hM3Dq-PBS and hM3Dq-CNO, respectively;,
192 p=0.0177; 3h body weight change, 0.5±0.04 g and -0.55±0.19 g for hM3Dq-PBS and hM3Dq-
193 CNO, respectively; p<0.0001, **Fig. 4a,b, Extended Data Fig. 5a**). In contrast, silencing BNC2
194 neurons during the light cycle significantly increased food consumption and body weight (3h food
195 intake: 0.15±0.03 g and 0.51±0.06 g for hM4Di-PBS and hM4Di-CNO, respectively; p=0.0008; 3h
196 body weight change, -0.16±0.08 g and 0.34±0.09 g for hM4Di-PBS and hM3Dq-CNO, respectively;
197 p=0.0002, **Fig. 4c,d**).
198 We next evaluated the dynamics of the feeding response using optogenetics[33]. AAVs with
199 Cre-dependent versions of the activating channeldhodopsin-2 (ChR2)-GFP or inhibitory soma-
200 targeted *Guillardia theta* anion-conducting channelrhodopsins (stGtACR2)-FusionRed were
201 injected into the ARC of BNC2-cre mice after which an optical fiber was implanted over the
202 ARC[33,34]. (**Fig. 4e, Extended Data Fig. 5b**). Optogenetic activation of BNC2 neurons at a

203 frequency of 20 Hz for 20 minutes led to a significant reduction in food intake in mice that were
204 fasted overnight compared to controls expressing GFP and the decreased food intake persisted
205 for up to 20 mins even after the cessation of light stimulation (**Fig. 4f**). Activating ARC BNC2
206 neurons did not affect locomotion (**Extended Data Fig. 5c**). Consistent with the results from
207 chemogenetic inhibition, optogenetic silencing of BNC2 neurons at 20 Hz significantly increased
208 food intake in mice during the light cycle but this did not persist when the photoinhibition ceased
209 (**Fig. 4g**).
210 We also used optogenetics to assess the effect of BNC2 neural activation on valence
211 using a real-time place preference assay (**Fig. 4h**). We found a significant preference of mice for
212 the chamber associated with BNC2 activation after an overnight fast compared to GFP expressing
213 controls (**Fig. 4i,j**). However, there was no preference for the photostimulation-paired chamber in
214 sated mice that were tested in the light cycle (**Fig. 4j, Extended Data Fig. 5d**). Food deprivation
215 leads to the activation of AGRP/NPY neurons which is associated with negative valence raising
216 the possibility that BNC2 activation is associated with positive valence because these neurons
217 inhibit AGRP/NPY neurons[21,35]. We evaluated this possibility by combining optogenetic activation
218 of BNC2 neurons with electrophysiologic recordings from AGRP/NPY neurons in hypothalamic
219 slices.
220
221 **BNC2 neurons monosynaptically inhibit AgRP/NPY neurons**
222 A Flp-dependent mCherry AAV (fDIO-mCherry) and a Cre-dependent ChR2-GFP AAV
223 (DIO-ChR2-GFP) were co-injected into the ARC of *BNC2-Cre*::*NPY-FlpO* mice[36]. We found dense
224 GFP expression in BNC2 terminals within the ARC, in proximity to the mCherry expressing
225 AGRP/NPY soma (**Fig. 5a**). This finding, the positive valence of BNC2 activation after fasting and
226 the observation that BNC2 neurons express Vgat (*Slc32a1*, **Fig. 1e,f**) raised the possibility that
227 BNC2 neurons might directly inhibit AGRP/NPY neurons. We evaluated this using ChR2-assisted
228 circuit mapping (CRACM) on brain slices[37,38]. Evoked inhibitory postsynaptic currents (oIPSCs)
229 were recorded in mCherry-labeled AGRP/NPY neurons before and after optogenetic activation of
230 BNC2 neurons (**Fig. 5b**). We found synchronized oIPSCs after light activation in approximately
231 81% of AGRP/NPY neurons (25/31) with a rapid onset and a latency of 5.12 millisecond (**Fig. 5c-**
232 **e**) indeed suggesting that BNC2 neurons directly inhibit AGRP/NPY neurons. Consistent with this,
233 the oIPSCs were abolished after the application of the sodium channel blocker tetrodotoxin (TTX),
234 which blocks action potential in all neurons, but inhibitory currents onto AGRP/NPY neurons were
235 restored by the co-application of 4-aminopyride (4-AP), a potassium channel antagonist that
236 enables ChR2-mediated depolarization of local presynaptic terminals (**Fig. 5c,f**). Finally, the

237 oIPSCs observed in the presence of TTX and 4-AP were blocked after the application of the
238 $GABA_A$ receptor antagonist picrotoxin (PTX) (**Fig. 5c,f**). In aggregate, these data show that BNC2
239 neurons directly inhibit AGRP/NPY neurons via the $GABA_A$ receptor.
240 We also tested whether AGRP/NPY neurons could inhibit BNC2 neurons by injecting AAV-
241 fDIO-ChR2-GFP and AAV-DIO-mCherry into the ARC of *BNC2-Cre*::*NPY-FlpO* mice. However, in
242 contrast to the effects of BNC2 activation to increase oIPSCs in AGRP/NPY neurons, we failed to
243 see an effect of AGRP/NPY activation on post-synaptic currents in mCherry labeled BNC2
244 neurons (0 out of 25) (**Fig. 5g-i**). This was despite the fact that brief blue light pulses triggered
245 action potentials in GFP-labeled AGRP/NPY neurons (**Extended Data Fig. 6**). Thus while BNC2
246 neurons directly inhibit AGRP/NPY neurons, AGRP/NPY neurons do not alter the activity BNC2
247 neurons.
248 Previous reports have shown that AGRP/NPY neuronal activity is inhibited by the
249 presence of food[21,35]. This raised the possibility that BNC2 neuronal activation might mediate
250 some or all of the effect of food cues to inhibit AGRP/NPY neurons. We tested this by injecting an
251 inhibitory DREADD, AAV-DIO-hM4Di-mCherry, together with an AAV-fDIO-GCamp6s into the
252 ARC of *BNC2-Cre*::*NPY-FlpO* (**Fig. 6a**). After an overnight fast, we administered PBS or CNO 30
253 minutes prior to providing the animal with chow (**Fig. 6b**). Consistent with the prior results (**Fig.
254 4**), inhibition of BNC2 neurons significantly increased food intake relative to PBS-treated controls
255 (**Fig. 6c**). We then imaged the activity of AGRP/NPY neurons after refeeding using fiber
256 photometry with or without inhibition of BNC2 neurons. As previously reported, control mice
257 receiving PBS showed a robust reduction in calcium signals in AGRP/NPY neurons when given
258 food (**Fig. 6d,e**). We then measured the activity of AGRP/NPY neurons after giving CNO and
259 found that the inhibition of BNC2 neurons significantly attenuated the decrease in AGRP/NPY
260 activity seen after refeeding (**Fig. 6d,e**). These findings suggest that a portion of the sensory
261 inputs that suppress AGRP/NPY neurons after refeeding are conveyed by BNC2 neurons.
262
263 **Deletion of leptin receptors in BNC2 neurons causes hyperphagia and obesity**
264 BNC2 neurons express the leptin receptor (**Fig. 1**) and are activated by leptin (**Fig. 2**)
265 suggesting that they mediate some of leptin's effects. We assess this by knocking out LepR in
266 BNC2 neurons using CRISPR-Cas9 genome editing technology. BNC2-Cre mice were bred to
267 LSL-Cas9-GFP mice[39], and an AAV carrying two single guide RNAs (sgRNAs) designed to target
268 the mouse *Lepr* (sgLepr) locus, or two control guide RNAs (sgCtrl)[23,40], were injected bilaterally
269 into the ARC. The specific deletion of the *Lepr* gene was confirmed by showing that leptin no
270 longer increased the levels of pSTAT3 in BNC2 neurons that received injections of the sgLepr

271 guide RNAs compared to those with sgCtrl guide RNAs (**Fig. 2, Extended Data Fig. 7**).

272 Mice with a LepR knockout in BNC2 neurons, gained significantly more weight compared
273 to the sgCtrl-injected mice (28.14±0.37g and 35.57±1.43g for sgCtrl and sgLepr, respectively;
274 p=0.0001, **Fig. 7a**). 8-weeks after the guide RNA injection, fat mass within the sgLepr group was
275 also significantly increased relative to the sgCtrl group with a small increase in lean mass (**Fig.**
276 **7b**). Daily food intake was significantly higher in sgLepr mice at week 8, compared to their sgCtrl
277 counterparts (4.27±0.21g and 5.24±0.28g for sgCtrl and sgLepr, respectively; p=0.0185, **Fig. 7c**).
278 Total energy expenditure (EE) was significantly increased in the BNC2 LepR knockout mice and
279 there was still a significant increase when it was indexed to lean mass (**Fig. 7d,e, Extended Data**
280 **Fig. 8a**)[41]. However, this difference was no longer significant when the regression analysis of EE
281 was calculated relative to body weight (**Extended Data Fig. 8b**). While the basis for the increased
282 expenditure is not known, this indicates that the primary effect of the knockout to increase weight
283 is a result of increased food intake. There was no difference in locomotor activity between the two
284 groups (**Extended Data Fig. 8c,d**). The respiratory exchange ratio (RER) was higher in the
285 sgLepr group in comparison to the sgCtrl group (**Extended Data Fig. 8e,f**), suggesting that there
286 is increased carbohydrate utilization. Finally, we assayed glucose tolerance and found that sgLepr
287 mice had increased fasting blood glucose levels (**Fig. 7f**). The BNC2 LepR knockout mice also
288 showed impaired glucose tolerance during a glucose tolerance test (GTT), and a significantly
289 reduced response to insulin compared to sgCtrl mice as demonstrated by the insulin tolerance
290 test (ITT) (**Fig. 7g,h**). While the impaired glucose tolerance is consistent with the increased
291 adiposity of the knockouts, the data do not exclude the possibility that these neurons directly
292 regulate glucose metabolism. Taken together, these findings show that leptin signaling to ARC
293 BNC2 plays a functional role to regulate food intake and body weight.
294

295 **Discussion**

296 Leptin is the afferent signal in a negative feedback loop regulating food intake and body
297 weight. Leptin regulates the activity of discrete neural populations expressing LepR in the ARC
298 and elsewhere[1]. In the ARC, leptin decreases the activity of orexigenic AGRP/NPY neurons and
299 activates anorexigenic neurons expressing POMC. However, several lines of evidence have
300 raised the possibility that there are additional, as yet unknown leptin-regulated neurons that
301 suppress appetite (see below)[13,14,42]. However, the nature of this putative population(s) was not
302 known.

303 Here, we report the use of snRNA-seq to identify a novel LepR-expressing neuron cluster
304 in the ARC that expresses the *Bnc2* marker gene. While there are fewer BNC2/LepR neurons

305 compared to those expressing POMC and AGRP, the level of LepR in BNC2 neurons is as high
306 or higher than in these other populations. The data further show that BNC2 neurons are rapidly
307 activated by leptin or the presence of food and that the level of activation is further modulated by
308 food palatability and nutritional status (**Extended Data Fig. 9**). BNC2/LepR neurons directly inhibit
309 AGRP/NPY neurons and BNC2 activation reduces food intake for a sustained period. Finally, in
310 contrast to anorexigenic POMC neurons, a BNC2-specific knockout of LepR causes significant
311 hyperphagia and obesity. These findings establish a role for BNC2 neurons to acutely induce
312 satiety and thus add an important new cellular component to the neural pathways that maintain
313 homeostatic control of energy balance.

314 The *Bnc2* gene encodes a conserved transcription factor that has been reported to play a
315 role in cell development, proliferation, pigmentation, and liver fibrosis[43-46]. In support of a potential
316 role to regulate weight, genome-wide association studies (GWAS) have consistently linked the
317 *Bnc2* gene to body mass index, fat distribution, and diabetes[47-49], although the underlying
318 mechanisms have not been previously explored. This together with the data reported here
319 suggests that *Bnc2* itself may play a role in the development or function of the BNC2/LepR
320 neurons we identified. Further studies knocking out the *Bnc2* gene exclusively in BNC2/LepR
321 neurons will be necessary to assess this possibility, currently underway. While the function of
322 BNC2 in hypothalamus has not been ascertained, these studies establish that it is a highly specific
323 marker for a novel population of cells expressing LepR. While LepR clusters not expressing
324 AGRP/NPY or POMC have been previously identified in other studies, TRH, the canonical marker
325 expressed in this cluster is also expressed in non-LepR clusters[26]. In contrast, in hypothalamus
326 BNC2 expression is restricted to LepR neurons making it an especially useful marker for probing
327 the function of the neurons in this cluster. This enabled us to establish an important role for these
328 neurons to regulate food intake and mediate leptin action.

329 The canonical "yin-yang" model of feeding regulation has emphasized the opposing roles
330 of POMC neurons (suppressing hunger) and AGRP/NPY neurons (promoting hunger)[2,10].
331 However, the characteristics of these neural populations are markedly different in several respects.
332 For instance, while acute activation of AGRP/NPY neurons, using either opto- or chemo-genetic
333 methods, rapidly induces feeding within minutes[3,4], POMC neurons function as slow-acting satiety
334 regulators, and opto- and chemo-genetic stimulation of POMC neurons only has a minimal effect
335 on acute food intake[4,5,50]. Furthermore, an AGRP-specific LepR knockout in adult mice results in
336 severe obesity but a knockout of LepR in adult POMC neurons has a significantly smaller effect
337 on food intake and body weight[23]. In contrast, mutations that alter melanocortin signaling including
338 POMC, the PCSK1/2 processing enzymes, and MC4R cause severe obesity while mutations that

339 alter signaling in AGRP/NPY neurons have not been reported to alter weight[8,15,51]. Finally, while
340 leptin injections acutely suppress food intake, particularly in ob/ob mice, the activity of AGRP/NPY
341 and POMC neurons is not significantly altered by acute leptin injection[11,12]. In aggregate, these
342 findings raise the possibility that there might be a missing leptin-regulated neuronal population
343 that acutely suppresses food intake. Consistent with this, a knockout of LepR in GABAergic
344 neurons had a greater effect than did a knockout of LepR in AGRP or POMC neurons[13]. The
345 identity of this "missing" GABAergic population was not known and the evidence reported here
346 showing that BNC2/LepR neurons rapidly suppress feeding suggests that they serve this function.
347 However, these data do not exclude the possibility that additional populations might also
348 contribute.

349 Optogenetic activation of BNC2 neurons potently reduces food intake for a sustained
350 period even after photoactivation has ceased. This is similar to the sustained effect of AGRP/NPY
351 neuronal activation which induces a sustained increase in food intake through the release of
352 neuropeptide Y[52,53]. The sustained satiety effect lasted at least 20 minutes and could potentially
353 persist even longer. Previous research indicates that sustained hunger after AGRP/NPY neuron
354 activation can extend up to 1 hour[52]. Furthermore, the duration of the satiety effect may be
355 influenced by the duration of BNC2 neuron activation, akin to the pattern observed with
356 AGRP/NPY neuron activation[52]. BNC2 neurons are GABAergic and directly inhibit AGRP/NPY
357 neurons via the $GABA_A$ receptor though, as is the case for other feeding neurons, it is possible
358 that neuropeptides also contribute. The snRNA-seq data shows expression of several putative
359 neuropeptides in BNC2 neurons including *Scg2, Chga,* and *Trh,* which have been implicated in
360 feeding control and energy balance[54-59]. Future studies will be necessary to determine whether in
361 addition to GABA, these neuropeptides mediate some of the effects of BNC2 neurons.

362 BNC2 neurons suppress appetite, at least in part, by directly inhibiting AGRP/NPY neurons
363 via monosynaptic connections. However, similar to POMC neurons, this interaction is not
364 reciprocal[60,61] as AGRP/NPY neurons do not appear to modulate the activity of BNC2 neurons.
365 Similar to AGRP/NPY neurons, BNC2 neurons are activated by sensory cues associated with
366 food. Thus, similar to AGRP/NPY neurons BNC2 neurons function as coincidence detectors for
367 both sensory and interoceptive inputs such as leptin. The rapid regulation of AGRP/NPY and
368 BNC2 neurons by food cues is likely mediated by associative sensory inputs, the precise source
369 of which is currently unknown. It is plausible that these sensory inputs synapse onto both BNC2
370 neurons and AGRP/NPY neurons, exerting distinct effects on these two neuronal populations. If
371 true, mapping the afferent inputs to both may reveal anatomic sites that convey associative
372 sensory inputs. Alternatively, the food cues may primarily target BNC2 neurons, which

373 subsequently relay the information to AGRP/NPY neurons. In support of the former, we find that
374 inhibiting BNC2 neurons only partially blunts the effect of food cues to suppress AGRP/NPY
375 activity suggesting both direct and indirect (via BNC2 neurons) pathways by which sensory inputs
376 suppress AGRP/NPY neurons. It has also been shown that while food cues can transiently
377 suppress AGRP/NPY activity, caloric content and consumption are required for a sustained
378 reduction in their activity[62]. This is also the case for BNC2 neurons because the level of BNC2
379 neuron activity is markedly reduced when the food is not accessible.

380 Conditions of energy deficit activate AGRP/NPY neurons eliciting the aversive feeling of
381 hunger. A recent study revealed that AGRP/NPY neurons stimulate appetite by "teaching" animals
382 that food or food cues can suppress the negative valence associated with hunger[63]. The rapid
383 reduction in the aversive effect of activating AGRP/NPY neurons by food cues eventually
384 enhances the incentive salience of these cues, thereby facilitating learning of food acquisition
385 tasks over time. Similar to AGRP/NPY neurons, the level of activation of BNC2 neurons is
386 dependent on food availability, the duration of its presence, food palatability, and energy state but
387 in contrast, BNC2 neuron activation is associated with positive valence. However, this response
388 is only evident after fasting when AGRP/NPY activity is high. This suggests that BNC2 activation
389 contributes to these learned responses and that food can both induce reward and suppress
390 negative valence in fasted mice.

391 Deletion of LepR in adult BNC2 neurons resulted in abnormal GTTs and ITTs, implying a
392 potential regulatory role of BNC2 neurons in glucose metabolism. The impaired glucose tolerance
393 and insulin action in BNC2 LepR knockout mice could be a secondary consequence of the
394 pronounced obesity that develops. However, it is also possible that BNC2 neurons may directly
395 fluence on glucose metabolism similar to the acute activation of AGRP/NPY neurons which
396 impairs systemic insulin sensitivity, independent of its effect to increase feeding[24]. Here again,
397 some of these effects could be a result of the effect of BNC2 neurons on AGRP/NPY neural activity.
398 We also found that despite increasing food intake and body weight, a LepR knockout in BNC2
399 neurons paradoxically increased energy expenditure though this was no longer significant when
400 it was corrected for body weight. This is in contrast to a global knockout of LepR in db/db mice
401 which show decreased energy expenditure and also reduced lean[64,65]. The basis for the increased
402 lean mass and EE in the BNC2 LepR knockouts is not known and suggests that other neural
403 pathways contribute to the reduced energy expenditure and lower lean mass associated with
404 defects in leptin signaling. The identification of the specific pathways responsible for this will
405 require further investigation as will an explanation for the increased energy expenditure in the

406 BNC2 LepR knockouts. In aggregate, the data suggest that the increased weight of the BNC2
407 LepR knockouts is a result of hyperphagia.
408 In summary, we have identified BNC2 neurons as a fast-acting population of neurons that
409 acutely regulate feeding and energy balance bidirectionally. These findings add an important new
410 component to the neural circuit that regulates appetite and adiposity, while also shedding new
411 light on the mechanisms by which leptin regulates this system. Finally, pharmacologic activation
412 of these neurons could have therapeutic implications to reduce weight or to suppress the negative
413 valence associated with hunger[66].
414
415 **Methods**
416 **Mice**
417 All animal experiments were approved by the Institutional Animal Care and Use Committee at
418 Rockefeller University and were carried out in accordance with the National Institutes of Health
419 guidelines. Mice were group housed in a 12-h light/12-h dark cycle at 22 °C and 30–60% humidity
420 with ad-libitum access to a regular chow diet and water. We used the following genotypes of mice:
421 C57BL/6J (wild type; number 000664, The Jackson Laboratory), NPY-IRES2-FlpO-D (The
422 Jackson Laboratory, stock no. 030211), Rosa26-LSL-Cas9 (The Jackson Laboratory, stock no.
423 024857), BNC2-P2A-iCre (made in-house). For all Cre or Flp mouse line experiments, only
424 heterozygous animals were used. Sample sizes were decided based on experiments from similar
425 studies. Littermates of the same sex were randomly assigned to either experimental or control
426 groups.
427
428 **Generation of BNC2-P2A-iCre mouse line**
429 The BNC2-P2A-iCre mouse line was generated by the CRISPR and Genome Editing Resource
430 Center and Transgenic and Reproductive Technology Resource Center at Rockefeller University
431 using CRISPR-Cas9 technology[29]. Briefly, a custom-designed long single-stranded DNA (lssDNA)
432 donor, containing homology arms of *Bnc2* locus flanking the P2A-iCre sequence, was inserted
433 near the endogenous STOP codon. Two guide RNAs (sgRNAs) were employed to induce site-
434 specific double-stranded breaks. The lssDNA donor with the pre-assembled Cas9 protein/gRNA
435 complexes was mixed and microinjected into C57BL/6J (The Jackson Laboratory) mouse zygotes
436 following standard CRISPR genome engineering protocols. The resulting live offspring were
437 genotyped through PCR with two sets of primers that specifically amplified the mutant allele.
438 Validation was ensured via Sanger sequencing. The BNC2-P2A-iCre transgenic animals were
439 bred to C57BL/6J mice for maintenance.

440

441 **Viruses**

442 AAV viruses used in these studies were obtained from Addgene, UNC Vector Core, or generated
443 through Janelia Viral Tools Service. We used the following viruses: AAV5-hSyn-DIO-hM3D(Gq)-
444 mCherry (Addgene, #44361, 2.2 × 10^{13} vg/mL), AAV5-hSyn-DIO-hM4Di(Gi)-mCherry (Addgene,
445 #44362, 2.5 × 10^{13} vg/mL), AAV5-hSyn-DIO-mCherry (Addgene, #50459, 2.2 × 10^{13} vg/mL),
446 AAV5-Ef1a-DIO-EYFP (Addgene, #27056, 1.6 × 10^{13} vg/mL), AAV5-hSyn-Flex-GCaMP6s-WPRE
447 (Addgene, #100845, 2.9 × 10^{13} vg/mL), AAV5-EF1a-DIO-hChR2(H134R)-EYFP (UNC Vector
448 Core, 2.7 × 10^{12} vg/mL), AAV1-hSyn1-SIO-stGtACR2-FusionRed (Addgene, #105677, 2.1 × 10^{13}
449 vg/mL), AAV5-Ef1a-fDIO-mCherry (Addgene, #114471, 2.3 × 10^{13} vg/mL), AAV8-Ef1a-fDIO-
450 GCamp6s (Addgene, #105714, 2.1 × 10^{13} vg/mL), AAV5&DJ-EF1a-fDIO-hChR2(H134R)-EYFP-
451 WPRE (UNC Vector Core, 1.4 × 10^{12} vg/mL). For *Lepr* deletion, AAV viral vectors were cloned in-
452 house and packaged with the AAV5 serotype through Janelia Viral Tools Service. The sequences
453 of sgLepR are: 5'-GAGTCATCGGTTGTGTTCGG-3', 5'-TGCCGGCGGTTGGATG GACT-3' (virus
454 titer, 4.9 × 10^{12} vg/mL); The sequence of sgCtrl is: 5'-TTTTTTTTTTTTTTGAATTC-3' (virus titer,
455 8.5 × 10^{12} vg/mL). Viral aliquots were stored at −80 °C before stereotaxic injection.

456

457 **Stereotactic surgery**

458 Mice (8–10 weeks old) were anesthetized using isoflurane anesthesia (induction 5%,
459 maintenance 1.5–2%) and positioned on a stereotaxic rig (Kopf Instruments, Model 1900).
460 Viruses were delivered into the brains through a glass capillary using a Drummond Scientific
461 Nanoject III Programmable Nanoliter Injector. For the ARC region, the following coordinates
462 relative to the bregma were used: anterior-posterior (AP), -1.65 mm to -1.70 mm; medial-lateral
463 (ML), ± 0.25 mm to 0.30 mm; and dorsal-ventral, (DV) -5.9 mm. For chemogenetics experiments,
464 Bnc2 neuron labeling, and *Lepr* deletion, 30-50 nl of the virus was injected bilaterally at a rate of
465 1 nl/s. For optogenetics, 30 nl of the virus was injected unilaterally at a rate of 1 nl/s followed by
466 the implant of an optical fiber (ThorLabs, CFM12U-20) at 200 μm above the ARC (AP: -1.65 mm,
467 ML: 0.3 mm, DV: -5.7 mm). For fiber photometry experiments, 30 nl of the virus was injected
468 unilaterally followed by the implant of an optical fiber cannula (Doric, MFP_400/430/1100-
469 0.57_1m_FCM-MF2.5_LAF) at 150 μm above the ARC (AP: -1.65 mm, ML: 0.3 mm, DV: -5.75
470 mm). For CRACM experiments, the two viruses were mixed at the ratio of 1:1, and 50 nl of the
471 mixed virus was injected bilaterally into the ARC.

472

473 **Isolation of nuclei and snRNA-seq**

474 Male C57BL/6J mice aged 10-12 weeks were euthanized via transcardial perfusion using ice-cold
475 HEPES-Sucrose Cutting Solution containing NaCl (110 mM), HEPES (10 mM), glucose (25 mM),
476 sucrose (75 mM), $MgCl_2$ (7.5 mM), and KCl (2.5 mM) at a PH of 7.4. Subsequently, brains were
477 quickly dissected in the same solution, frozen using liquid nitrogen, and stored at -80 °C until
478 nuclei isolation. To isolate nuclei, as previously described, the samples were thawed on ice,
479 resuspended in HD buffer containing tricine KOH (10 mM), KCl (25 mM), $MgCl_2$ (5 mM), sucrose
480 (250 mM), 0.1% Triton X-100, SuperRNaseIn (0.5 U/ml), RNase Inhibitor (0.5 U/ml).
481 Homogenization was performed using a 1-ml dounce homogenizer. The resulting homogenates
482 were filtered using a 40 μM filter, centrifuged at 600g for 10 minutes, and resuspended in nucleus
483 storage buffer containing sucrose (166.5 mM), $MgCl_2$ (10 mM), Tris buffer (pH 8.0, 10 mM),
484 SuperRNaseIn (0.05 U/ml), RNase Inhibitor (0.05 U/ml) for subsequent staining. Nucleus quality
485 and number were assessed using an automated cell counter (Countess II, Thermo Fisher). For
486 staining, nuclei were labeled with Hoechst 33342 (Thermo Scientific H3570; 0.5 μl per million
487 nuclei), anti-NeuN Alexa Fluor 647-conjugated antibody (Abcam ab190565) (0.5 μl per million
488 nuclei), and TotalSeq anti-Nuclear Pore Complex Proteins Hashtag antibody (BioLegend 682205)
489 (0.5 mg per million nuclei) for 15 minutes at 4 °C. Following staining, samples were washed with
490 10 ml 2% BSA (in PBS) and centrifuged at 600g for 5 minutes. Nuclei were then resuspended in
491 2% BSA (in PBS) with RNase inhibitors (SuperRNaseIn 0.5 U/ml, RNase Inhibitor 0.5 U/ml) for
492 subsequent fluorescence-activated cell sorting. The samples were gated based on Hoechst
493 fluorescence to identify nuclei and then further sorted based on high Alexa Fluor 647 expression,
494 designating NeuN+ nuclei as neurons.
495 Nuclei were captured and barcoded using 10x Genomics Chromium v3 following the
496 manufacturer's protocol. The processing and library preparation were carried out by the Genomics
497 Resource Center at Rockefeller University, and sequencing was performed by Genewiz using
498 Illumina sequencers.
499
500 **SnRNA-seq analysis**
501 The FASTQ file was analyzed with Cell Ranger version 5.0. The snRNA-seq data for ARC (WT)
502 was preprocessed individually using the Seurat v4 (v4.0.3). Cells with more than 800 and fewer
503 than 5,000 RNA features were selected for further analysis. Cells with greater than 1%
504 mitochondrial genes and greater than 12,000 total RNA counts were also removed. Genes
505 detected in fewer than 3 cells were excluded. Then we demultiplexed the cells based on their
506 hashtag count (positive. quantile =0.8) using the built-in function in Seurat v4. Only the cells with
507 singlet Hashtag assignment were kept for downstream analysis. The data was then log-

508 normalized with a scale factor of 10,000. After the initial quality control, demultiplexing, and
509 normalization steps, all the singlets were then scaled, and dimensionally reduced with PCA and
510 UMAP. Leiden clustering (resolution =0.55) was applied to identify clusters. We used known cell-
511 type specific gene expression to annotate the clusters. The analytic code and processed data are
512 available upon request.
513 Co-expression analysis of marker genes within the human ARC was performed using previously
514 published human adult samples and the data can be accessed through the NeMO archive
515 (https://assets.nemoarchive.org/dat-917e9vs). A cell was considered to express the marker gene
516 if at least 2 unique molecular identifiers (UMIs) were detected. The identification of arcuate cells
517 was achieved through clustering and the expression of canonical markers, as detailed in the
518 earlier study. Co-expression of genes like *Lepr*, *Bnc2*, *Agrp*, *Npy*, and *Pomc* was tabulated in R,
519 and two-tailed Fisher's tests were calculated to assess the significance of co-expression of gene
520 pairs within the 16,819 arcuate cells in the human dataset.
521
522 **Chemogenetics for activation or inhibition**
523 AAV viruses were bilaterally delivered into the ARC of male BNC2-iCre mice aged 8-10 weeks.
524 Mice were then allowed to recover and express DREADDs for at least 3 weeks. For activation or
525 inhibition, animals were intraperitoneally injected with 3 mg/kg of CNO or PBS (control).
526
527 **Optogenetics for activation or inhibition**
528 AAV viruses were unilaterally delivered into the ARC of male BNC2-iCre mice aged 8-10 weeks
529 followed by the implantation of an optic fiber. Subsequently, the mice were given a recovery period
530 of at least 3 weeks to allow for gene expression. Prior to the experiments, the mice were
531 habituated to patch cables over a period of 5 days. The implanted optic fibers were connected to
532 patch cables using ceramic sleeves (Thorlabs) and linked to a 473 nm laser (OEM
533 Lasers/OptoEngine, Midvale, UT). The output of the laser was verified at the beginning of each
534 experiment. A blue light, generated by a 473 nm laser diode (OEM Lasers/OptoEngine) with a
535 power of 15 mW, was used. The light pulse (10 ms) and frequency (20 Hz) were controlled through
536 a waveform generator (Keysight) to either activate or inhibit Bnc2 neurons in the ARC. In the
537 activation feeding experiments, mice were allowed to acclimate to the cage for 20 minutes.
538 Subsequently, three feeding sessions, each lasting 20 minutes, were initiated. During these
539 sessions, the light was turned off for the initial 20 minutes, switched on for the subsequent 20
540 minutes, and then turned off again for the remaining 20 minutes. In the inhibition feeding
541 experiments, following the 20-minute acclimation, each feeding session was extended to 30

542 minutes. The amount of food consumed during each feeding session was manually recorded.
543 Animals were sacrificed at the end of the experiments to confirm viral expression and fiber
544 placement using immunohistochemistry.
545
546 **Real-time place preference**
547 A custom-made 2-chamber box (50 × 50 × 25 cm black plexiglass) with an 8.5 cm gap enabling
548 animals to move freely between the chambers is used for this assay. To evaluate the mice's initial
549 preference, they were introduced into the box for a 10-minute session without any
550 photostimulation. Subsequently, in the second 10-minute session following the initial one,
551 photostimulation (15 mW, 20 Hz) was paired with the chamber that the mice exhibited less
552 preference for during the initial session. The Ethovision software, coupled with a CCD camera,
553 facilitated the recording of the percentage of time spent by the mice in each chamber.
554
555 **Fiber photometry**
556 Mice were acclimated to tethering and a home cage-style arena for 5 minutes daily over the
557 course of 5 days prior to the experiment. Data acquisition was conducted using a Fiber
558 Photometry system from Tucker-Davis Technologies (RZ5P, Synapse) and Doric components,
559 with recordings synchronized to video data in Ethovision through TTL triggering. A dual
560 fluorescence Mini Cube (Doric) combined light from 465nm and isosbestic 405nm LEDs, which
561 were transmitted via the recording fiber connected to the implant. GCaMP6s fluorescence,
562 representing the calcium-dependent signal (525nm), and isosbestic control (430nm) were
563 detected using femtowatt photoreceivers (Newport, 2151) and a lock-in amplifier at a sampling
564 rate of 1kHz. Analysis was conducted using a Matlab script involving the removal of bleaching
565 and movement artifacts through a polynomial least square fit applied to the 405nm signal,
566 adjusting it to the 465nm trace (405_{fitted}), and then calculating the GCaMP signal as % $\Delta F/F =$
567 $(465_{signal}-405_{fitted})/405_{fitted}$. The resulting traces were filtered using a moving average filter and
568 down-sampled by a factor of 20. The code is available upon request.
569
570 **In situ hybridization**
571 Mice were briefly transcardially perfused with ice-code RNase-free PBS. Brains were then quickly
572 collected, embedded in OCT on dry ice, and stored at −80°C until cryostat sectioning (15 μm
573 thickness) onto Superfrost Plus Adhesion Slides (Thermo Fisher). RNAscope Fluorescent
574 Multiplex assay (Advanced Cell Diagnostics Bio) was performed based on the manufacturer's
575 protocol. All reagents were purchased from Advanced Cell Diagnostics (ACDbio). Probes for the

576 following mRNAs were used: Agrp (cat no. 400711-C3), Pomc (cat no. 314081-C3), Lepr (cat no.
577 402731), Slc31a1 (cat no. 319191), Bnc2 (cat no. 518521-C2). Briefly, brain sections were fixed
578 in 4% PFA at 4°C for 15 minutes followed by serial submersion in 50% EtOH, 70% EtOH, and
579 twice in 100% EtOH for 5 minutes each at room temperature. Sections were treated with Protease
580 IV for 30 minutes at RT followed by a 2-hour incubation with specific probes at 40°C using a
581 HyBez oven. Signal amplification was achieved through successive incubations with Amp-1, Amp-
582 2, Amp-3, and Amp-4 for 30, 15, 30, and 15 minutes, respectively, at 40°C using a HyBez oven.
583 Each incubation step was followed by two 2-minute washes in RNAscope washing buffer. Nucleic
584 acids were counterstained with DAPI Fluoromount-G (SouthernBiotech) mounting medium before
585 coverslipping. The slides were visualized using an inverted Zeiss LSM 780 laser scanning
586 confocal microscope with a ×20 lens. The acquired images were imported into Fiji for further
587 analysis.
588
589 **Immunohistochemistry**
590 Mice were transcardially perfused with PBS first and then 4% PFA for fixation. Brains were
591 collected and immersed in 4% PFA overnight at 4°C for additional fixation. Fixed brains were
592 sequentially immersed in 10% sucrose, 20% sucrose, and 30% sucrose buffers for 1 hour, 1 hour,
593 and overnight, respectively, all at 4°C. After this, the brains were embedded in OCT and stored at
594 -80°C until cryostat sectioning (30-50 μm thickness). For the staining process, brain sections were
595 first blocked in a blocking buffer containing 3% BSA, 2% goat serum, and 0.1% triton X-100 in
596 PBS for 30 minutes at room temperature followed by an overnight incubation with primary
597 antibodies in the cold room. After washing in PBS, the sections were incubated with fluorescence-
598 conjugated secondary antibodies (Invitrogen) for 1h at room temperature. Stained sections were
599 mounted onto SuperFrost (Fisher Scientific 22-034- 980) slides and then visualized with an
600 inverted Zeiss LSM 780 laser scanning confocal microscope with a ×10 or ×20 lens. The acquired
601 images were imported to Fiji for further analysis. The following antibodies were used: cFos
602 antibody (1:1000, Synaptic systems, #226308), pSTAT3 antibody (1: 1000, Cell Signaling
603 Technology, #9145s), GFP (1:1000, abcam, ab13970), RFP (1:1000, Rockland, #600-401-379).
604
605 **Electrophysiology and channelrhodopsin-assisted circuit mapping (CRACM)**
606 Adult mice were euthanized via transcardial perfusion using ice-cold cutting solution containing
607 choline chloride (110 mM), $NaHCO_3$ (25 mM), KCl (2.5 mM), $MgCl_2$ (7 mM), $CaCl_2$ (0.5 mM),
608 NaH_2PO4 (1.25 mM), glucose (25 mM), ascorbic acid (11.6 mM), and pyruvic acid (3.1 mM).
609 Subsequently, brains were quickly dissected in the same solution and sectioned through a

610 vibratome into 275 μm coronal sections. These sections were then incubated in artificial cerebral
611 spinal fluid containing NaCl (125 mM), KCl (2.5 mM), NaH_2PO_4 (1.25 mM), $NaHCO_3$ (25 mM),
612 $MgCl_2$ (1 mM), $CaCl_2$ (2 mM), and glucose (11 mM) at 34 °C for 30 minutes, followed by room
613 temperature incubation until use. The intracellular solution for current-clamp recordings contained
614 K-gluconate (145 mM), $MgCl_2$ (2 mM), Na_2ATP (2 mM), HEPES (10 mM), EGTA (0.2
615 mM, 286 mOsm, pH 7.2). The intracellular solution for the voltage clamp recording contained
616 $CsMeSO_3$ (135 mM), HEPES (10 mM), EGTA (1 mM), QX-314 (chloride salt, 3.3 mM), Mg-ATP
617 (4 mM), Na-GTP (0.3 mM), and sodium phosphocreatine (8 mM, pH 7.3 adjusted with CsOH).
618 Signals were acquired using the MultiClamp 700B amplifier and digitized at 20 kHz using
619 DigiData1550B (Molecular Devices). The recorded electrophysiological data were analyzed using
620 Clampfit (Molecular Devices) and MATLAB (Mathworks).
621 For CRACM experiments, voltage-clamp recordings were conducted on Bnc2 and Npy neurons.
622 To record oIPSCs, the cell membrane potential was held at 0 mV. ChR2-expressing axons were
623 activated using brief pulses of full-field illumination (0.5 ms, 0.1 Hz, 10 times) onto the recorded
624 cell with a blue LED light (pE-300 white; CoolLED). Subsequently, TTX (1 μM), 4-AP (100 mM),
625 and PTX (1 μM) were sequentially applied through the bath solution, each for 10–20 minutes.
626 Data acquisition commenced at least 5 minutes after each drug application.
627
628 **Indirect calorimetry**
629 Indirect calorimetry was performed using the Phenomaster automated home cage phenotyping
630 system (TSE Systems, Bad Homburg, Germany). Mice were individually housed in
631 environmentally controlled chambers maintained at 22°C, following a 12-h light/12-h dark, and at
632 40% humidity, with ad libitum access to food and water. O_2 and CO_2 measurements were collected
633 at 15-minute intervals with a settling time of 3 minutes and a sample flow rate of 0.25 L/minute.
634 The raw data obtained were analyzed using CalR[41].
635
636 **Blood glucose, glucose, and insulin tolerance test**
637 Blood glucose levels were measured using a OneTouch Ultra meter and glucose test strips. For
638 glucose tolerance tests (GTT), mice were fasted overnight followed by a 20% glucose injection
639 (2 g/kg) and glucose measurements at 0, 15, 30, 60, and 120 minutes. Insulin tolerance tests (ITT)
640 were conducted after a 4-hour fast, with insulin injection (0.75 U/kg) and glucose measurements
641 at 0, 15, 30, 45, 60, and 120 minutes.
642
643 **Statistical analysis**

All statistical analyses were performed in GraphPad Prism 9. Data distribution was tested for normality (Shapiro-Wilk test) and then comparisons were made using parametric or non-parametric tests, as appropriate. Two-tailed statistical tests were used, and statistical significance was determined by Student's t-test, Mann-Whitney test, Fisher's exact test, one-way or 2-way ANOVA, and Friedman test as indicated in the Source Data.

Data availability

All data generated or analyzed during this study are included in the manuscript and supporting files. The raw sequencing data have been deposited in the Gene Expression Omnibus and are available under the accession number GSE249564. The processed data are available upon request.

Code availability

The analytic code is available upon request.

References

1 Friedman, J. M. Leptin and the endocrine control of energy balance. *Nat Metab* **1**, 754-764 (2019). https://doi.org:10.1038/s42255-019-0095-y

2 Andermann, M. L. & Lowell, B. B. Toward a Wiring Diagram Understanding of Appetite Control. *Neuron* **95**, 757-778 (2017). https://doi.org:10.1016/j.neuron.2017.06.014

3 Krashes, M. J. *et al.* Rapid, reversible activation of AgRP neurons drives feeding behavior in mice. *J Clin Invest* **121**, 1424-1428 (2011). https://doi.org:10.1172/JCI46229

4 Aponte, Y., Atasoy, D. & Sternson, S. M. AGRP neurons are sufficient to orchestrate feeding behavior rapidly and without training. *Nat Neurosci* **14**, 351-355 (2011). https://doi.org:10.1038/nn.2739

5 Zhan, C. *et al.* Acute and long-term suppression of feeding behavior by POMC neurons in the brainstem and hypothalamus, respectively. *J Neurosci* **33**, 3624-3632 (2013). https://doi.org:10.1523/JNEUROSCI.2742-12.2013

6 Zhang, Y. *et al.* Positional cloning of the mouse obese gene and its human homologue. *Nature* **372**, 425-432 (1994). https://doi.org:10.1038/372425a0

7 Baldini, G. & Phelan, K. D. The melanocortin pathway and control of appetite-progress and therapeutic implications. *J Endocrinol* **241**, R1-R33 (2019). https://doi.org:10.1530/JOE-18-0596

8 Yeo, G. S. H. *et al.* The melanocortin pathway and energy homeostasis: From discovery to obesity therapy. *Mol Metab* **48**, 101206 (2021). https://doi.org:10.1016/j.molmet.2021.101206

9 Cowley, M. A. *et al.* Leptin activates anorexigenic POMC neurons through a neural network in the arcuate nucleus. *Nature* **411**, 480-484 (2001). https://doi.org:10.1038/35078085

10 Gautron, L., Elmquist, J. K. & Williams, K. W. Neural control of energy balance: translating circuits to therapies. *Cell* **161**, 133-145 (2015). https://doi.org:10.1016/j.cell.2015.02.023

685 11 Mistry, A. M., Swick, A. G. & Romsos, D. R. Leptin rapidly lowers food intake and elevates
686 metabolic rates in lean and ob/ob mice. *J Nutr* **127**, 2065-2072 (1997).
687 https://doi.org:10.1093/jn/127.10.2065
688 12 Beutler, L. R. *et al.* Dynamics of Gut-Brain Communication Underlying Hunger. *Neuron* **96**,
689 461-475 e465 (2017). https://doi.org:10.1016/j.neuron.2017.09.043
690 13 Vong, L. *et al.* Leptin action on GABAergic neurons prevents obesity and reduces
691 inhibitory tone to POMC neurons. *Neuron* **71**, 142-154 (2011).
692 https://doi.org:10.1016/j.neuron.2011.05.028
693 14 Rupp, A. C. *et al.* Specific subpopulations of hypothalamic leptin receptor-expressing
694 neurons mediate the effects of early developmental leptin receptor deletion on energy
695 balance. *Mol Metab* **14**, 130-138 (2018). https://doi.org:10.1016/j.molmet.2018.06.001
696 15 Lindberg, I. & Fricker, L. D. Obesity, POMC, and POMC-processing Enzymes: Surprising
697 Results From Animal Models. *Endocrinology* **162** (2021).
698 https://doi.org:10.1210/endocr/bqab155
699 16 Ste Marie, L., Luquet, S., Cole, T. B. & Palmiter, R. D. Modulation of neuropeptide Y
700 expression in adult mice does not affect feeding. *Proc Natl Acad Sci U S A* **102**, 18632-
701 18637 (2005). https://doi.org:10.1073/pnas.0509240102
702 17 Erickson, J. C., Clegg, K. E. & Palmiter, R. D. Sensitivity to leptin and susceptibility to
703 seizures of mice lacking neuropeptide Y. *Nature* **381**, 415-421 (1996).
704 https://doi.org:10.1038/381415a0
705 18 Corander, M. P., Rimmington, D., Challis, B. G., O'Rahilly, S. & Coll, A. P. Loss of agouti-
706 related peptide does not significantly impact the phenotype of murine POMC deficiency.
707 *Endocrinology* **152**, 1819-1828 (2011). https://doi.org:10.1210/en.2010-1450
708 19 Luquet, S., Perez, F. A., Hnasko, T. S. & Palmiter, R. D. NPY/AgRP neurons are essential
709 for feeding in adult mice but can be ablated in neonates. *Science* **310**, 683-685 (2005).
710 https://doi.org:10.1126/science.1115524
711 20 Gropp, E. *et al.* Agouti-related peptide-expressing neurons are mandatory for feeding. *Nat*
712 *Neurosci* **8**, 1289-1291 (2005). https://doi.org:10.1038/nn1548
713 21 Betley, J. N. *et al.* Neurons for hunger and thirst transmit a negative-valence teaching
714 signal. *Nature* **521**, 180-185 (2015). https://doi.org:10.1038/nature14416
715 22 Qu, N. *et al.* A POMC-originated circuit regulates stress-induced hypophagia, depression,
716 and anhedonia. *Mol Psychiatry* **25**, 1006-1021 (2020). https://doi.org:10.1038/s41380-
717 019-0506-1
718 23 Xu, J. *et al.* Genetic identification of leptin neural circuits in energy and glucose
719 homeostases. *Nature* **556**, 505-509 (2018). https://doi.org:10.1038/s41586-018-0049-7
720 24 Steculorum, S. M. *et al.* AgRP Neurons Control Systemic Insulin Sensitivity via Myostatin
721 Expression in Brown Adipose Tissue. *Cell* **165**, 125-138 (2016).
722 https://doi.org:10.1016/j.cell.2016.02.044
723 25 Gaublomme, J. T. *et al.* Nuclei multiplexing with barcoded antibodies for single-nucleus
724 genomics. *Nat Commun* **10**, 2907 (2019). https://doi.org:10.1038/s41467-019-10756-2
725 26 Campbell, J. N. *et al.* A molecular census of arcuate hypothalamus and median eminence
726 cell types. *Nat Neurosci* **20**, 484-496 (2017). https://doi.org:10.1038/nn.4495
727 27 Steuernagel, L. *et al.* HypoMap-a unified single-cell gene expression atlas of the murine
728 hypothalamus. *Nat Metab* **4**, 1402-1419 (2022). https://doi.org:10.1038/s42255-022-
729 00657-y
730 28 Yao, Z. *et al.* A high-resolution transcriptomic and spatial atlas of cell types in the whole
731 mouse brain. *bioRxiv* (2023). https://doi.org:10.1101/2023.03.06.531121
732 29 Shola, D. T. N., Yang, C., Han, C., Norinsky, R. & Peraza, R. D. Generation of Mouse
733 Model (KI and CKO) via Easi-CRISPR. *Methods Mol Biol* **2224**, 1-27 (2021).
734 https://doi.org:10.1007/978-1-0716-1008-4_1

30 Buettner, C. *et al.* Critical role of STAT3 in leptin's metabolic actions. *Cell Metab* **4**, 49-60 (2006). https://doi.org:10.1016/j.cmet.2006.04.014

31 Minatohara, K., Akiyoshi, M. & Okuno, H. Role of Immediate-Early Genes in Synaptic Plasticity and Neuronal Ensembles Underlying the Memory Trace. *Front Mol Neurosci* **8**, 78 (2015). https://doi.org:10.3389/fnmol.2015.00078

32 Roth, B. L. DREADDs for Neuroscientists. *Neuron* **89**, 683-694 (2016). https://doi.org:10.1016/j.neuron.2016.01.040

33 Emiliani, V. *et al.* Optogenetics for light control of biological systems. *Nature Reviews Methods Primers* **2**, 55 (2022). https://doi.org:10.1038/s43586-022-00136-4

34 Mahn, M. *et al.* High-efficiency optogenetic silencing with soma-targeted anion-conducting channelrhodopsins. *Nat Commun* **9**, 4125 (2018). https://doi.org:10.1038/s41467-018-06511-8

35 Chen, Y., Lin, Y. C., Kuo, T. W. & Knight, Z. A. Sensory detection of food rapidly modulates arcuate feeding circuits. *Cell* **160**, 829-841 (2015). https://doi.org:10.1016/j.cell.2015.01.033

36 Daigle, T. L. *et al.* A Suite of Transgenic Driver and Reporter Mouse Lines with Enhanced Brain-Cell-Type Targeting and Functionality. *Cell* **174**, 465-480 e422 (2018). https://doi.org:10.1016/j.cell.2018.06.035

37 Rost, B. R., Wietek, J., Yizhar, O. & Schmitz, D. Optogenetics at the presynapse. *Nat Neurosci* **25**, 984-998 (2022). https://doi.org:10.1038/s41593-022-01113-6

38 Petreanu, L., Huber, D., Sobczyk, A. & Svoboda, K. Channelrhodopsin-2-assisted circuit mapping of long-range callosal projections. *Nat Neurosci* **10**, 663-668 (2007). https://doi.org:10.1038/nn1891

39 Platt, R. J. *et al.* CRISPR-Cas9 knockin mice for genome editing and cancer modeling. *Cell* **159**, 440-455 (2014). https://doi.org:10.1016/j.cell.2014.09.014

40 Wang, P. *et al.* A leptin-BDNF pathway regulating sympathetic innervation of adipose tissue. *Nature* **583**, 839-844 (2020). https://doi.org:10.1038/s41586-020-2527-y

41 Mina, A. I. *et al.* CalR: A Web-Based Analysis Tool for Indirect Calorimetry Experiments. *Cell Metab* **28**, 656-666 e651 (2018). https://doi.org:10.1016/j.cmet.2018.06.019

42 Leshan, R. L., Greenwald-Yarnell, M., Patterson, C. M., Gonzalez, I. E. & Myers, M. G., Jr. Leptin action through hypothalamic nitric oxide synthase-1-expressing neurons controls energy balance. *Nat Med* **18**, 820-823 (2012). https://doi.org:10.1038/nm.2724

43 Vanhoutteghem, A. *et al.* Basonuclin 2 has a function in the multiplication of embryonic craniofacial mesenchymal cells and is orthologous to disco proteins. *Proc Natl Acad Sci U S A* **106**, 14432-14437 (2009). https://doi.org:10.1073/pnas.0905840106

44 Romano, R. A., Li, H., Tummala, R., Maul, R. & Sinha, S. Identification of Basonuclin2, a DNA-binding zinc-finger protein expressed in germ tissues and skin keratinocytes. *Genomics* **83**, 821-833 (2004). https://doi.org:10.1016/j.ygeno.2003.11.009

45 Bobowski-Gerard, M. *et al.* Functional genomics uncovers the transcription factor BNC2 as required for myofibroblastic activation in fibrosis. *Nat Commun* **13**, 5324 (2022). https://doi.org:10.1038/s41467-022-33063-9

46 Vanhoutteghem, A. *et al.* The importance of basonuclin 2 in adult mice and its relation to basonuclin 1. *Mech Dev* **140**, 53-73 (2016). https://doi.org:10.1016/j.mod.2016.02.002

47 Paterson, A. D. *et al.* A genome-wide association study identifies a novel major locus for glycemic control in type 1 diabetes, as measured by both A1C and glucose. *Diabetes* **59**, 539-549 (2010). https://doi.org:10.2337/db09-0653

48 Pant, S. D. *et al.* Comparative Analyses of QTLs Influencing Obesity and Metabolic Phenotypes in Pigs and Humans. *PLoS One* **10**, e0137356 (2015). https://doi.org:10.1371/journal.pone.0137356

49 Rask-Andersen, M., Karlsson, T., Ek, W. E. & Johansson, A. Genome-wide association study of body fat distribution identifies adiposity loci and sex-specific genetic effects. *Nat Commun* **10**, 339 (2019). https://doi.org:10.1038/s41467-018-08000-4

50 Koch, M. *et al.* Hypothalamic POMC neurons promote cannabinoid-induced feeding. *Nature* **519**, 45-50 (2015). https://doi.org:10.1038/nature14260

51 Loos, R. J. F. & Yeo, G. S. H. The genetics of obesity: from discovery to biology. *Nat Rev Genet* **23**, 120-133 (2022). https://doi.org:10.1038/s41576-021-00414-z

52 Chen, Y. *et al.* Sustained NPY signaling enables AgRP neurons to drive feeding. *Elife* **8** (2019). https://doi.org:10.7554/eLife.46348

53 Krashes, M. J., Shah, B. P., Koda, S. & Lowell, B. B. Rapid versus delayed stimulation of feeding by the endogenously released AgRP neuron mediators GABA, NPY, and AgRP. *Cell Metab* **18**, 588-595 (2013). https://doi.org:10.1016/j.cmet.2013.09.009

54 Mitchell, K. *et al.* Secretoneurin is a secretogranin-2 derived hormonal peptide in vertebrate neuroendocrine systems. *Gen Comp Endocrinol* **299**, 113588 (2020). https://doi.org:10.1016/j.ygcen.2020.113588

55 Trebak, F. *et al.* A potential role for the secretogranin II-derived peptide EM66 in the hypothalamic regulation of feeding behaviour. *J Neuroendocrinol* **29** (2017). https://doi.org:10.1111/jne.12459

56 Zhang, X. & van den Pol, A. N. Thyrotropin-releasing hormone (TRH) inhibits melanin-concentrating hormone neurons: implications for TRH-mediated anorexic and arousal actions. *J Neurosci* **32**, 3032-3043 (2012). https://doi.org:10.1523/JNEUROSCI.5966-11.2012

57 Schuhler, S. *et al.* Thyrotrophin-releasing hormone decreases feeding and increases body temperature, activity and oxygen consumption in Siberian hamsters. *J Neuroendocrinol* **19**, 239-249 (2007). https://doi.org:10.1111/j.1365-2826.2006.01524.x

58 Chavez, J. *et al.* Hypothalamic TRH mediates anorectic effects of serotonin in rats. *eNeuro* **9** (2022). https://doi.org:10.1523/ENEURO.0077-22.2022

59 Bandyopadhyay, G. K. & Mahata, S. K. Chromogranin A Regulation of Obesity and Peripheral Insulin Sensitivity. *Front Endocrinol (Lausanne)* **8**, 20 (2017). https://doi.org:10.3389/fendo.2017.00020

60 Roseberry, A. G., Liu, H., Jackson, A. C., Cai, X. & Friedman, J. M. Neuropeptide Y-mediated inhibition of proopiomelanocortin neurons in the arcuate nucleus shows enhanced desensitization in ob/ob mice. *Neuron* **41**, 711-722 (2004). https://doi.org:10.1016/s0896-6273(04)00074-1

61 Atasoy, D., Betley, J. N., Su, H. H. & Sternson, S. M. Deconstruction of a neural circuit for hunger. *Nature* **488**, 172-177 (2012). https://doi.org:10.1038/nature11270

62 Su, Z., Alhadeff, A. L. & Betley, J. N. Nutritive, Post-ingestive Signals Are the Primary Regulators of AgRP Neuron Activity. *Cell Rep* **21**, 2724-2736 (2017). https://doi.org:10.1016/j.celrep.2017.11.036

63 Berrios, J. *et al.* Food cue regulation of AGRP hunger neurons guides learning. *Nature* **595**, 695-700 (2021). https://doi.org:10.1038/s41586-021-03729-3

64 Bates, S. H. *et al.* LRb-STAT3 signaling is required for the neuroendocrine regulation of energy expenditure by leptin. *Diabetes* **53**, 3067-3073 (2004). https://doi.org:10.2337/diabetes.53.12.3067

65 Suriano, F. *et al.* Novel insights into the genetically obese (ob/ob) and diabetic (db/db) mice: two sides of the same coin. *Microbiome* **9**, 147 (2021). https://doi.org:10.1186/s40168-021-01097-8

66 Schneeberger, M. *et al.* Pharmacological targeting of glutamatergic neurons within the brainstem for weight reduction. *Nat Metab* **4**, 1495-1513 (2022). https://doi.org:10.1038/s42255-022-00677-8

Acknowledgments:

We thank all members of the laboratory of J.M.F. for discussions and support, Hong Duan from the Genomics Resource Center, and Flow Cytometry Resource Center for technical assistance with snRNA-seq experiments; Chingwen Yang from CRISPR and Genome Editing Center for generating the BNC2-P2A-iCre mouse line; and Bio-Imaging Resource Center. This work was supported by the JPB Foundation and the Howard Hughes Medical Institute (to J.M.F.) and the Kavli Neural Systems Institute Postdoctoral Fellowship (to H.L.T).

Author contributions:

H.L.T. conceived, designed, performed, and analyzed the research with inputs from all authors. L.Y. performed electrophysiology experiments and analyzed the data. Y.T. and P.W. analyzed the mouse snRNA-seq data. J.I., K.P., and A.I. performed experiments. B.R.H. analyzed the human snRNA-seq data. P.C. and D.L. provided inputs on experimental design. C.K. provided the code for fiber photometry data analysis. H.L.T. and J.M.F. wrote the manuscript.

Competing interests:

The authors declare no competing interests.

Materials & Correspondence:

Correspondence to Jeffrey M. Friedman

Fig.1: Identification of novel LepR-expressing neurons in the ARC

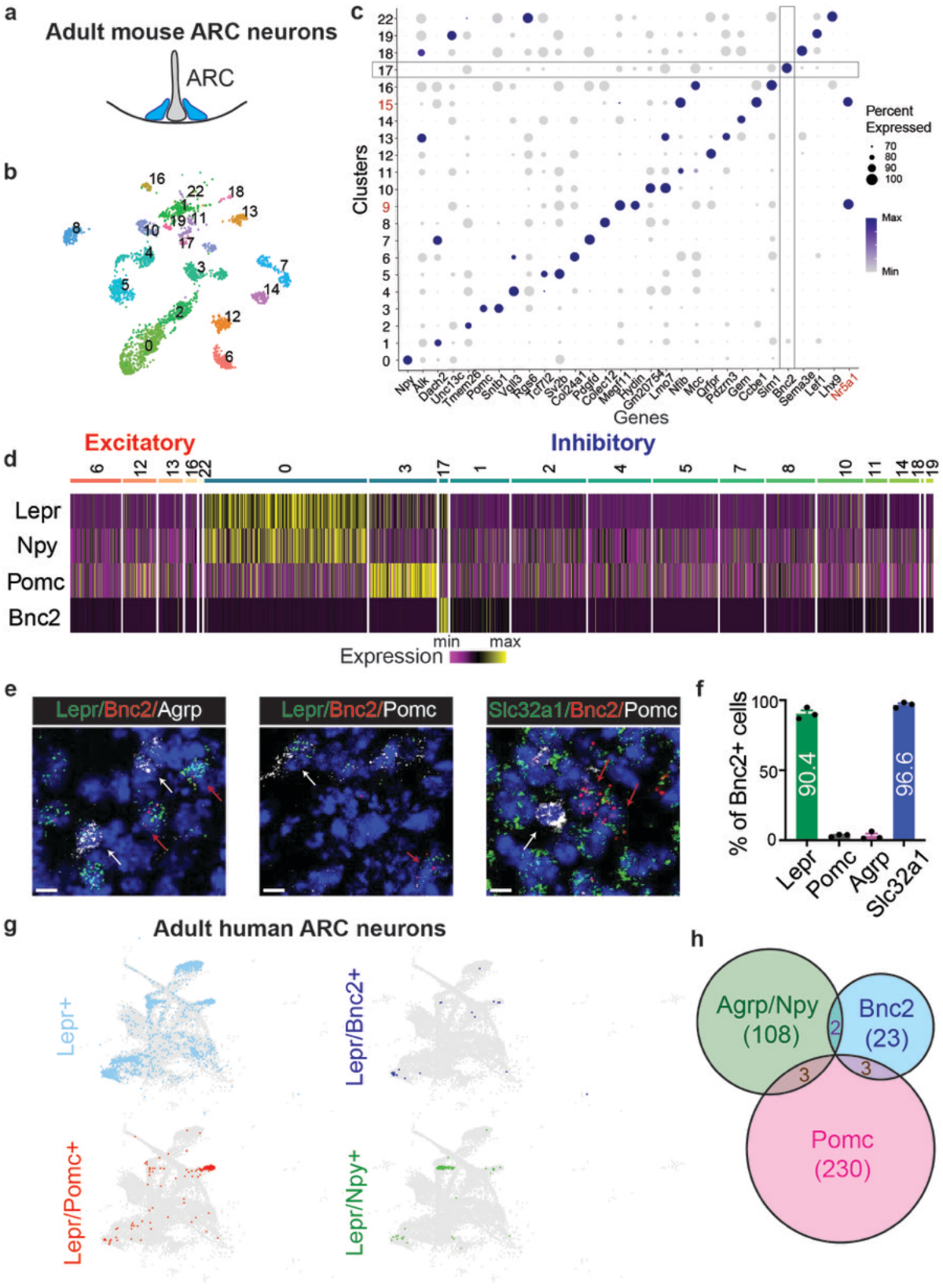

Fig. 1: Identification of novel LepR-expressing neurons in the ARC. a, Micro-dissection of mouse ARC. **b,** A uniform manifold approximation and projection (UMAP) plot of neuronal nuclei from the ARC (N = 6 adult male WT mice). **c,** Dot plot of maker genes of individual neuronal clusters and *Nr5a1* gene. **d,** Heatmap to plot the expression of indicated genes across individual clusters. Clusters were categorized into excitatory (*Slc17a6* positive) and inhibitory (*Slc321a*/*Gad1*/*Gad2* positive) neurons. **e,** RNA ISH against *Lepr*, *Bnc2*, *Agrp*, *Pomc*, *Slc32a1* in ARC of adult male WT mice. White arrow: *Agrp or Pomc positive* cells; Red arrow: *Bnc2 positive* cells. Scale bar, 10 μm. **f,** Percentage of *Bnc2*-positive cells co-expressing *Lepr*, *Pomc*, *Agrp*, and *Slc32a1* (N = 3 mice). **g,** UMAP plots of *Lepr*/*Pomc*, *Lepr*/*Bnc2*, and *Lepr*/*Npy* neurons in adult human ARC neurons. **h,** Colocalization of *Lepr*/*Bnc2*, *Lepr*/*Agrp*/*Npy*, and *Lepr*/*Pomc* neurons in adult human ARC neurons. Data are presented as mean ± SEM.

Fig.2: Activation of BNC2 neurons by leptin and feeding

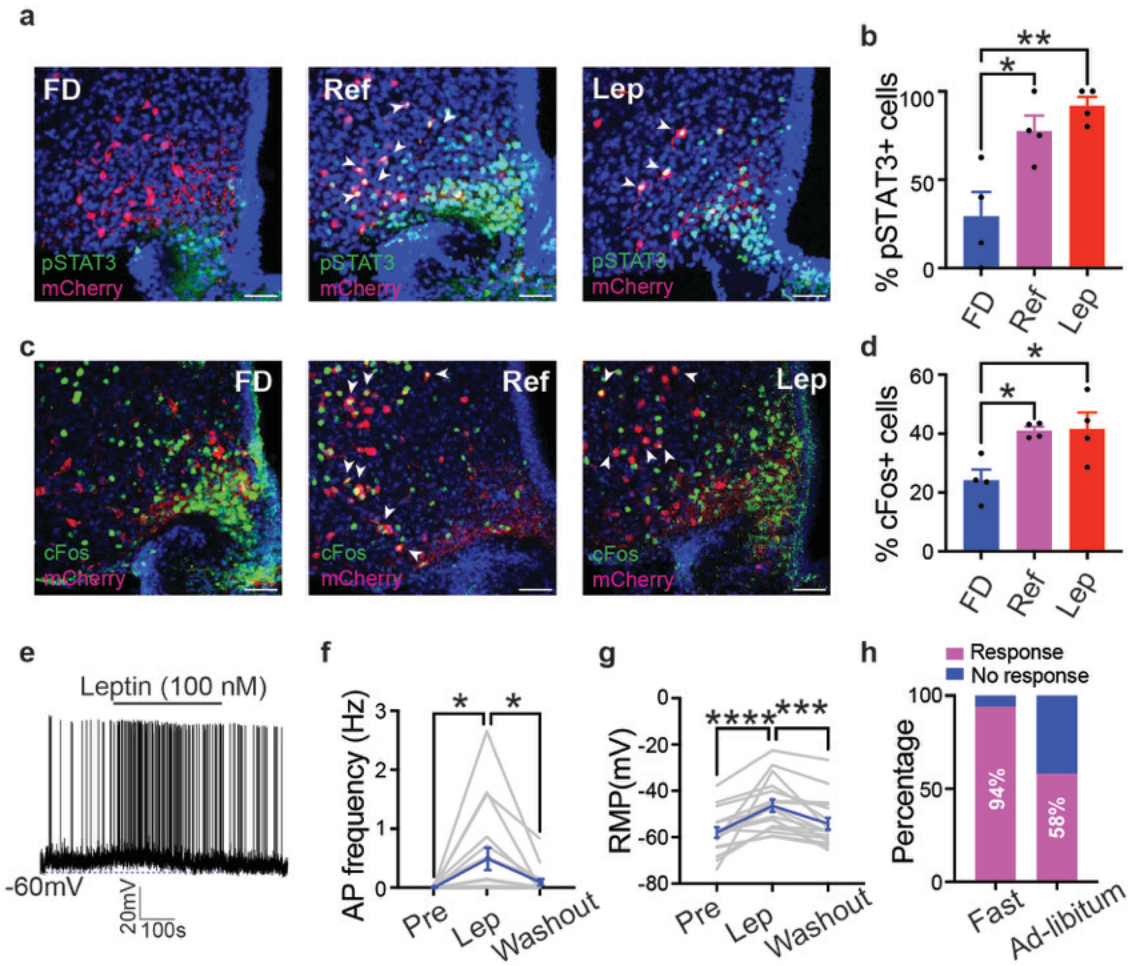

Fig. 2: Activation of BNC2 neurons by leptin and feeding. a,c, Brain slices from adult male BNC2-Cre mice, injected with DIO-mCherry into ARC, were subjected to pSTAT3 (**a**) and cFos (**c**) immunostaining under three conditions: overnight fasting (FD), overnight fasting followed by refeeding with chow for 3 hours (Ref), and overnight fasting followed by leptin injection (3mg/kg) for 3 hours (Lep). Scale bar, 50μm. **b,d,** Percentage of pSTAT3/mCherry double-positive cells (**b**) or cFos/mCherry double-positive cells (**d**) in mCherry positive cells (N = 4 mice per group). **e,** Spontaneous APs of BNC2 neurons in ARC from overnight fasted adult male BNC2-Cre mice (injected with DIO-GFP). Leptin (100 nM) was added to the bath solution at the indicated time window. **f,g,** Spontaneous AP frequency (**f**) and RMP (**g**) of BNC2 neurons before, during, and after leptin application (N = 17 cells from 4 mice per group). **h**, Percentage of leptin-responsive BNC2 neurons under the overnight fasting condition and ad-libitum-fed condition. Data are presented as mean ± SEM. *p<0.05; **p<0.01; ***p<0.001; ****p<0.0001. Details of the statistical analysis are provided as Source Data.

Fig. 3: Rapid responses of BNC2 neurons to food cues

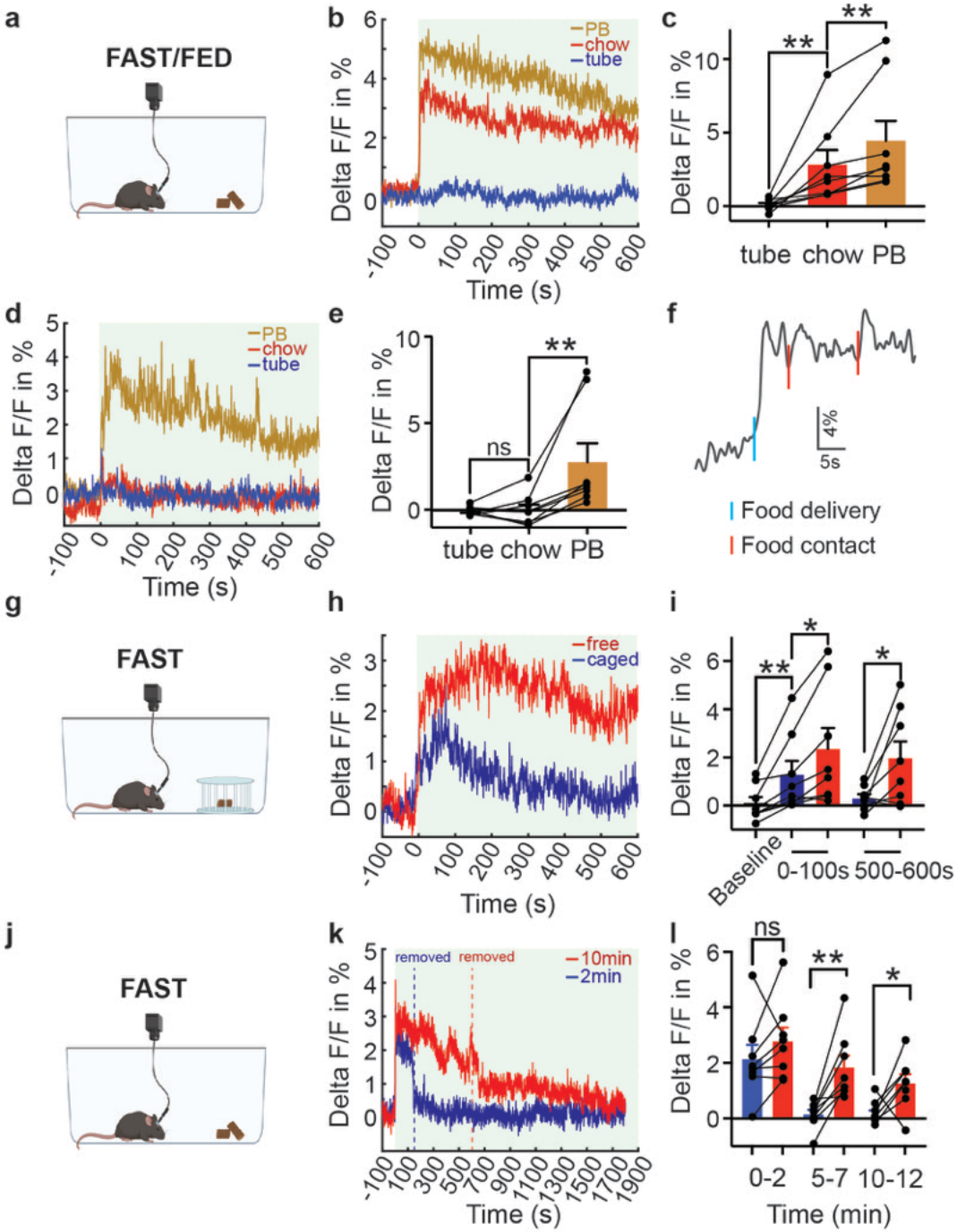

Fig.3: Rapid responses of BNC2 neurons to food cues. a-f, Recordings from mice expressing GCaMP6s in BNC2 neurons presented with an inedible plastic tube, chow, or peanut butter (PB). **b,** Average traces of calcium signals in fasted mice aligned to the time of presentation. **c,** Quantification of fluorescence changes within 0-300 second timeframe in b (N = 8 mice per group). **d,** Average traces in ad-libitum-fed mice aligned to the time of presentation. **e,** Quantification of fluorescence changes within 0-300 second timeframe in d (N = 8 mice per group). **f,** Individual trace of one overnight fasted mouse presented with PB. **g-i,** Recordings from overnight fasted mice presented with a chow inside or outside the container. **h,** Average traces aligned to the time of presentation. **i,** Quantification of fluorescence changes within 0-100 second and 500-600 second timeframes in h (N = 8 mice per group). **j-l,** Recordings from overnight fasted mice presented with a chow for 2 minutes or 10 minutes. **k,** Average traces aligned to the time of presentation. **l,** Quantification of fluorescence changes in the indicated timeframes in **k** (N = 8 mice per group). Data are presented as mean ± SEM. ns, not significant; *p<0.05; **p<0.01. Details of the statistical analysis are provided as Source Data.

Fig.4: Rapid and sustained satiety driven by BNC2 neurons

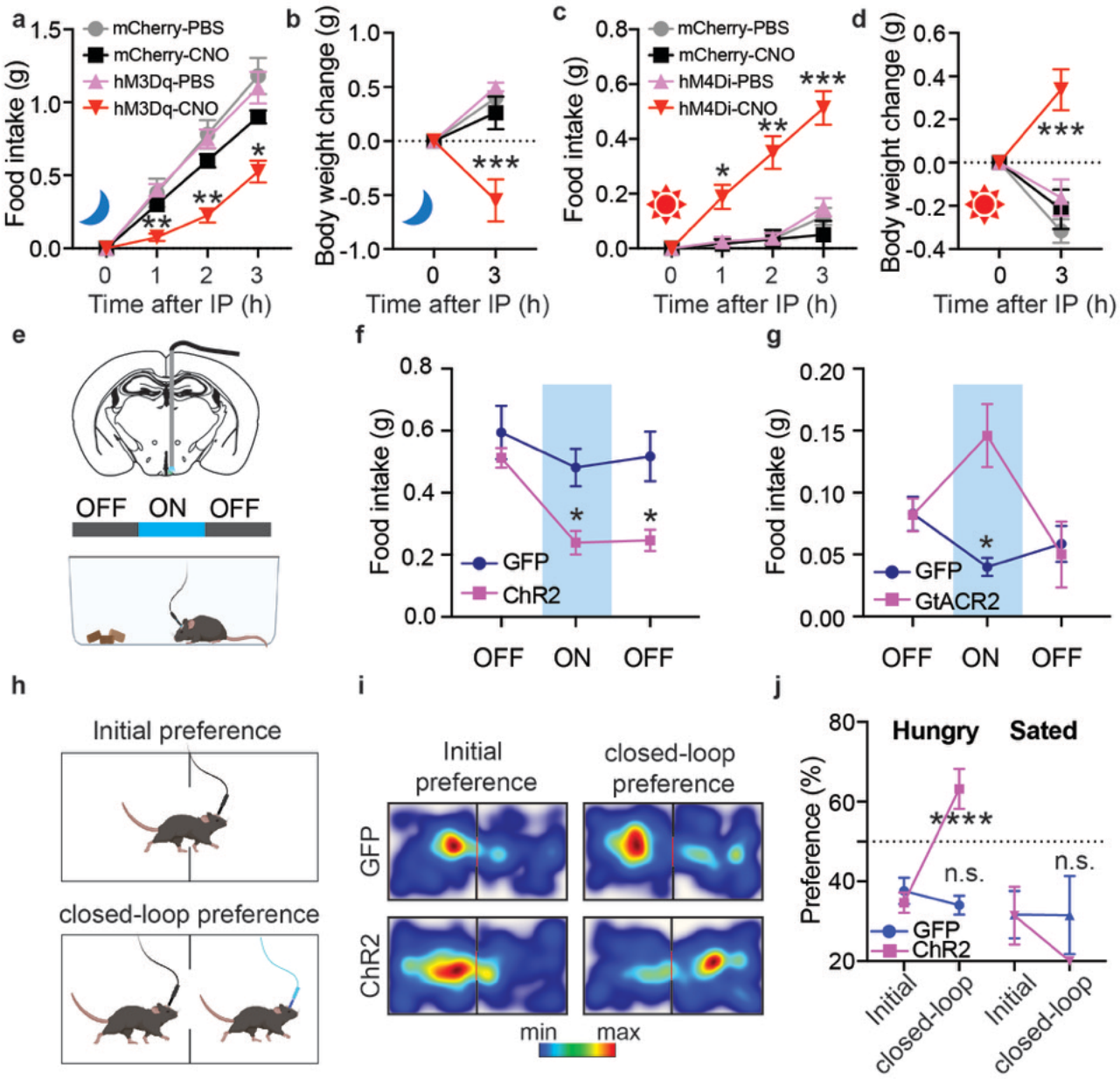

Fig. 4: Rapid and sustained satiety driven by BNC2 neurons. a, b, Hourly food intake (**a**) and body weight change at 3 hours (**b**) of each group of mice receiving PBS or CNO injection upon entering the night dark phase (N = 5 mCherry-injected mice, N = 4 hM3Dq-injected mice). **c, d,** Hourly food intake (**c**) and body weight change at 3 hours (**d**) of each group of mice receiving PBS or CNO injection in the daytime (N = 6 mCherry-injected mice, N = 8 hM4Di-injected mice). **e,** Unilateral injection of AAV viruses into the ARC region of adult male BNC2-Cre mice followed by fiber optic implant. **f,** Food intake of mice before, during, and after the activation of laser stimulation in overnight-fasted mice (N = 7 GFP-injected mice, N = 12 ChR2-injected mice). **g,** Food intake of mice before, during, and after the activation of laser stimulation in ad-libitum-fed mice in the daytime (N = 7 GFP-injected mice, N = 5 GtACR2-injected mice). **h-j,** Closed-loop place preference assay to assess the valence of BNC2 neurons. **i,** Heatmaps of time spent in each chamber of overnight fasted adult male BNC2-Cre mice injected with GFP or ChR2 during the initial phase and the closed-loop paired phase. **j,** Quantification of place preference (time spent in the pair-stimulated chamber, N = 6 GFP-injected mice, N = 8 ChR2-injected mice). ns, not significant; *p<0.05; **p<0.01; ***p<0.001; ****p<0.0001. Details of the statistical analysis are provided as Source Data.

Fig.5: BNC2 neurons monosynaptically inhibit NPY neurons

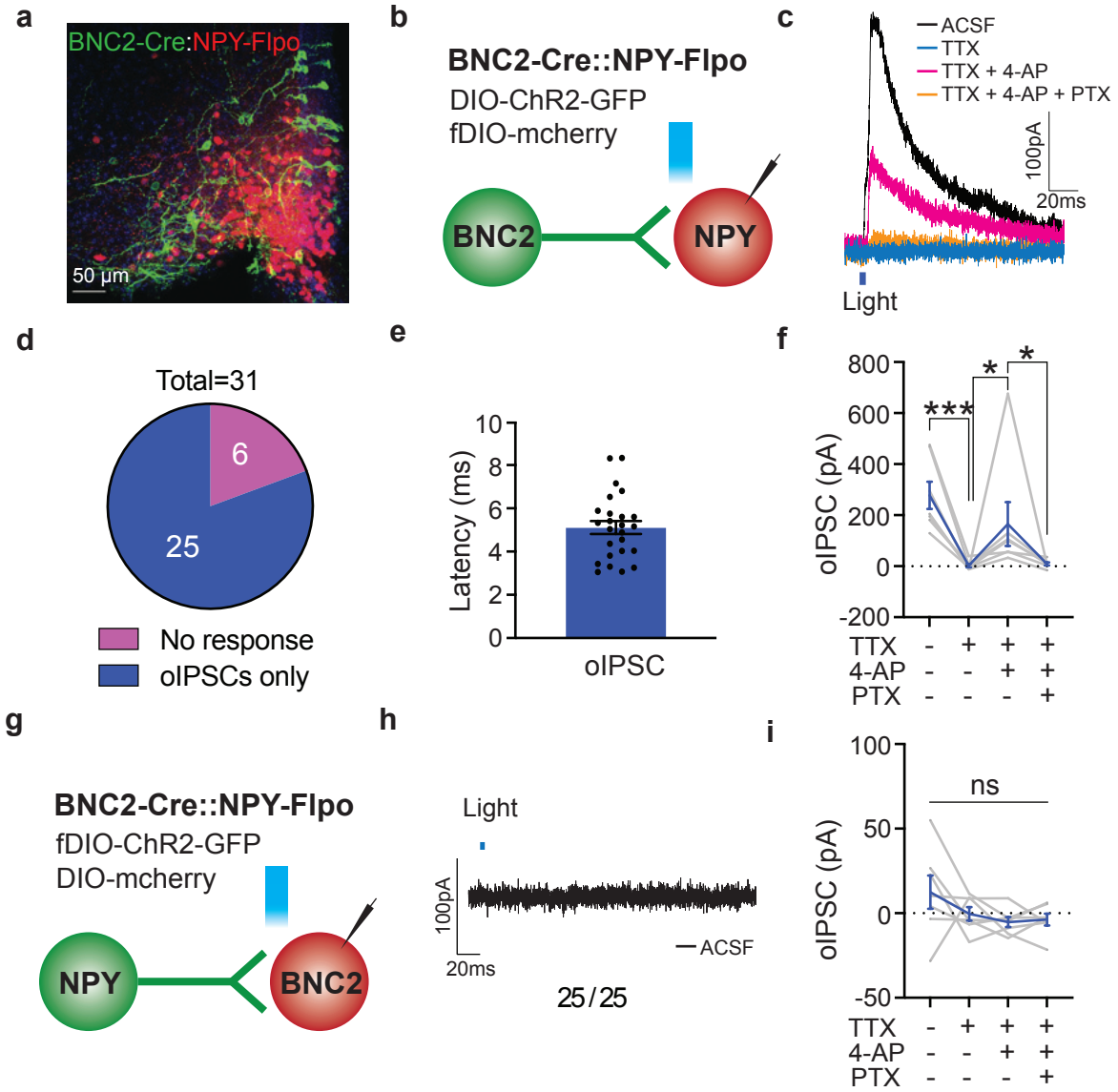

Fig. 5: BNC2 neurons monosynaptically inhibit NPY neurons. a, Immunostaining of GFP and mCherry in ARC from adult BNC2-Cre::NPY-Flpo mice injected with DIO-ChR2-GFP and fDIO-mCherry. Scale bar, 50 μm. **b,g,** Schematics of ChR2-assisted circuity mapping of the connections between BNC2 neurons and NPY neurons. **c,** Representative oIPSCs from NPY neurons following activation of BNC2 neurons with different blockers. **d,** Percentage of responsive NPY neurons (oIPSCs detected) following BNC2 neuron activation. **e,** oIPSC latency upon light stimulation (N = 29 cells from 4 mice). **f,** Quantification of oIPSC amplitude in c (N = 7 cells from 4 mice). **h,** Representative oIPSCs from BNC2 neurons following activation of NPY neurons. **i,** Quantification of oIPSC amplitudes in different conditions (N = 7 cells from 4 mice). ns, not significant; *p<0.05; ***p<0.001. Details of the statistical analysis are provided as Source Data.

Fig.6: BNC2 neurons mediate the regulation of food cues on NPY neuron activity

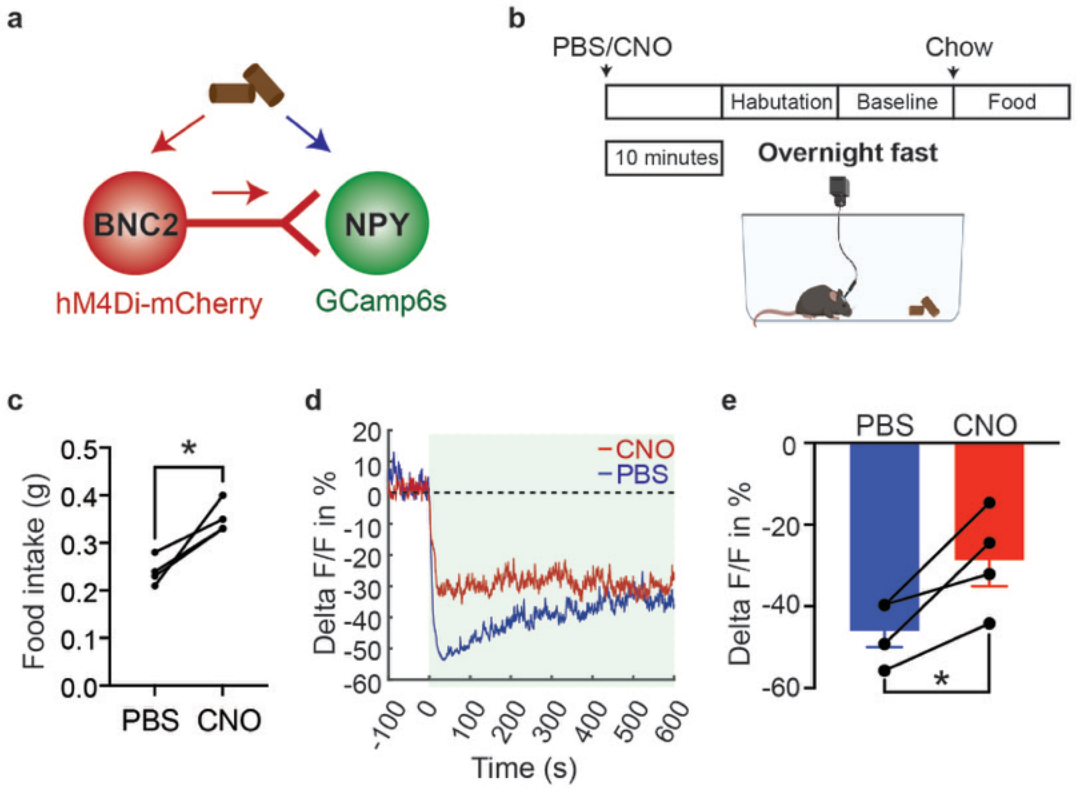

Fig. 6: BNC2 neurons mediate the regulation of food cues on NPY neuron activity. a, The experimental design and hypothesis. **b,** Schematic of PBS or CNO administration time during fiber photometry recordings of NPY neuron activity. **c,** Food consumption during the 10 minutes after food presentation in mice injected with PBS or CNO (N = 4 mice). **d,** Average traces of calcium signals from NPY neurons aligned to the time of presentation of chow in mice receiving PBS (blue) or CNO (red). **e,** Quantification of fluorescence changes within 0-200 second timeframe in d (N = 4 mice). Data are presented as mean ± SEM. ns, not significant; *p<0.05. Details of the statistical analysis are provided as Source Data.

Fig.7: LepR knockout in BNC2 neurons causes hyperphagia and obesity

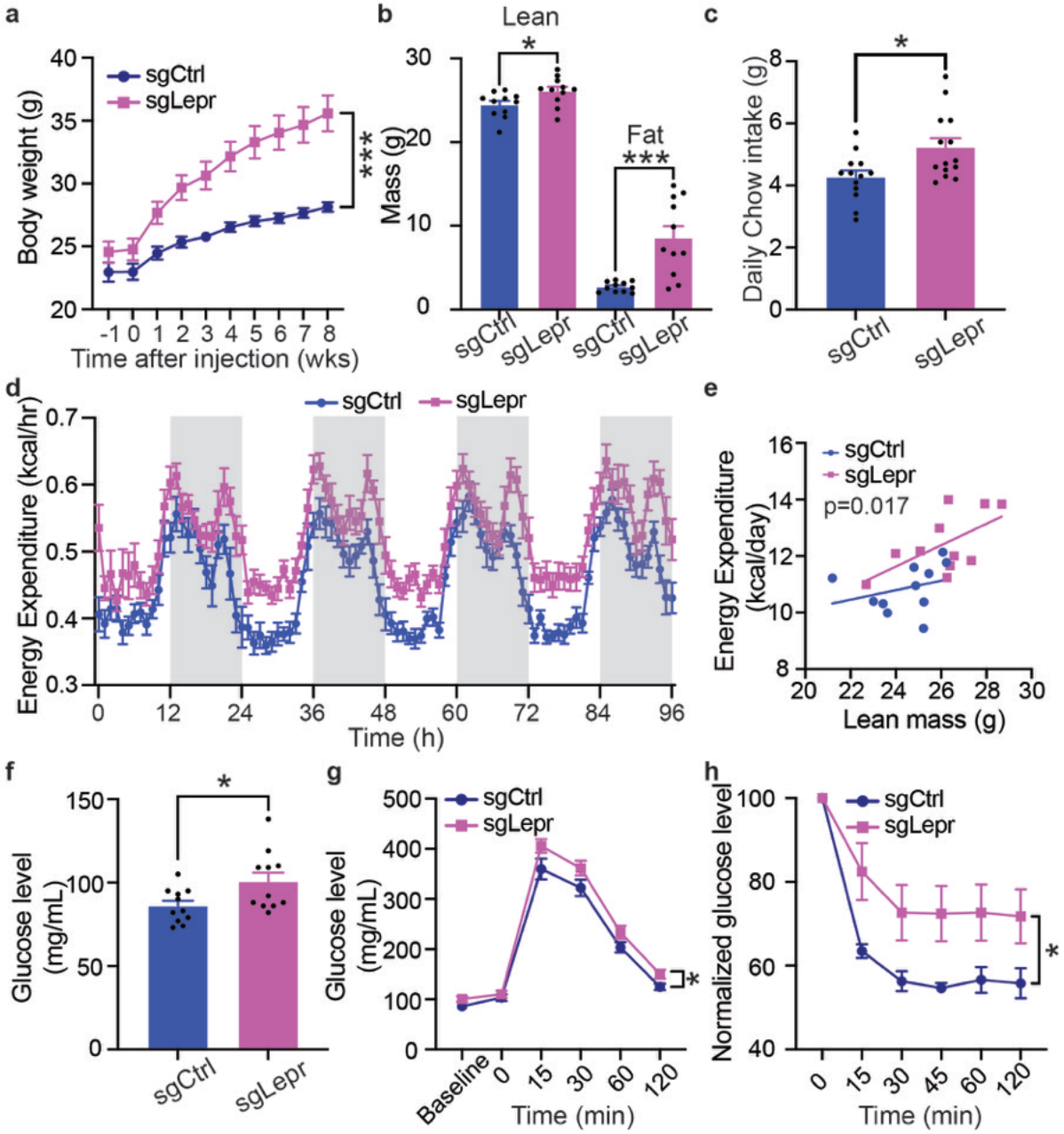

Fig.7: LepR knockout in BNC2 neurons causes hyperphagia and obesity. a, Body weight of mice fed on chow following injection of sgCtrl or sgLepr (N = 14 mice per group). **b,** Body composition of two groups of mice 8 weeks after virus injection (N = 11 mice per group). **c,** Daily chow intake of two groups at 8 weeks after virus injection (N = 13 sgCtrl-injected mice, N = 14 sgLepr-injected mice). **d,** Energy expenditure (EE) of two groups measured by indirect calorimetry at 10-12 weeks after virus injection. **e,** Regression analysis of EE vs. lean mass from d (N = 11 mice per group). **f,** Glucose levels of two groups after 16 h overnight fasting (N = 11 mice per group). **g,** Glucose tolerance test (GTT) of the two groups of mice at 10-12 weeks post virus injection (N = 11 mice per group). **h,** Insulin tolerance test (ITT) of the two groups of mice at 10-12 weeks post virus injection (N = 6 mice per group). Data are presented as mean ± SEM. ns, not significant; *p<0.05; ***p<0.001. Details of the statistical analysis are provided as Source Data.

Extended Data Fig.1: SnRNA-seq analysis of mouse ARC neurons

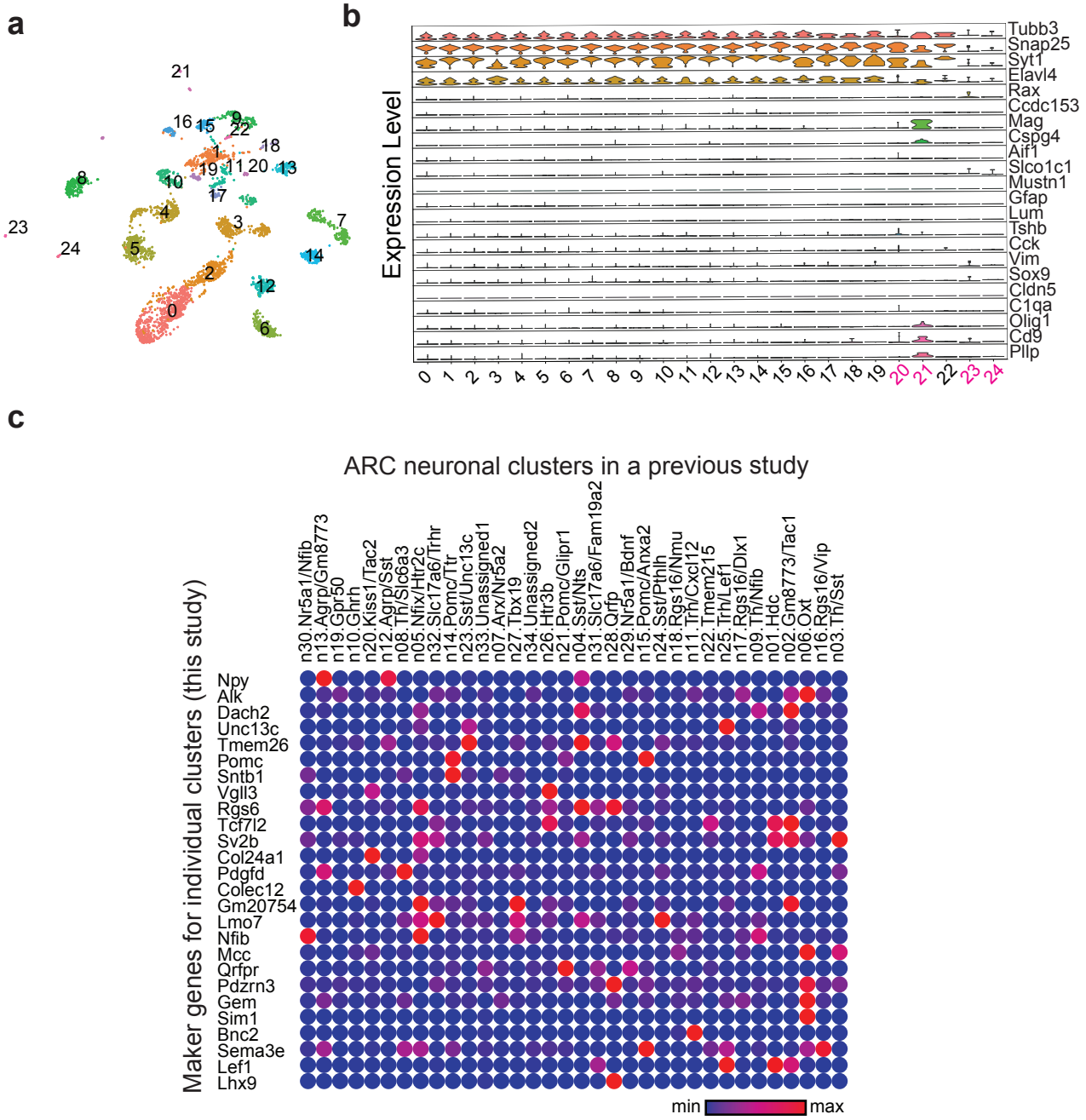

Extended Data Fig. 1: SnRNA-seq analysis of mouse ARC neurons. a, Single-cell UMAP plot of the ARC (N = 6 adult male WT mice). **b,** Violin plot of known markers of different cell types: neurons (Tubb3, Snap25, Syt1, Elavl4), tanycytes (Rax), ependymocytes (Ccdc153), oligodendrocyte cells (Mag, Olig1, Cspg4, Cd9, Pllp), macrophages (Aif1, C1qa), endothelial cells (Slco1c1, Cldn5), mural cells (Mustn1), astrocyte (Gfap, Sox9), vascular and leptomeningeal cells (Lum), pituitary cells (Tshb), pars tuberalis cells (Cck), ependymal cells (Vim). Clusters 20/21/23/24 are non-neuronal clusters. **c,** Dot plot displaying the expression of cluster-specific marker genes (identified in this study) across neuronal clusters with the ARC from a previous study[26].

Extended Data Fig.2: Generation of BNC2-P2A-iCre knockin mouse line

a

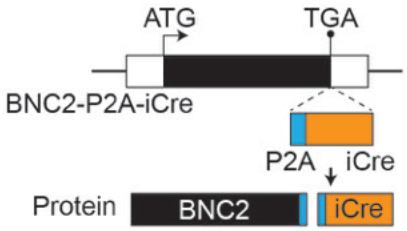

b **gRNAs used for gene editing:**
gRNA1: GGACTAATCTATTGAAGTGAAGG
gRNA2: TCAATAGATTAGTCCCAGAACGG

IssDNA template sequence:
acctgaatgggtacgggagaggcatggcagaggactacatggtccttgacctgagtaccacctccagcctccagtccagcagcagtgtccattcctccagag
agtccgatgcaggcagcgatgaggggattcttctcgacgacatcgatggcgcgagtgacagtggggaatccactcacaaggccgaggcccccaccctccc
cggcagcctcggggctgaagtttcaggatctcttatgttcagcagtttgtctgggagcaatggtgggatcatgtgcaacatttgccacaaaatgtacagcaacaa
ggggaccctgcgggtccactacaaaactgtgcatttgcgagagatgcataagtgcaaagtccccggctgtaacatgatgttctcctctgtgcgaagccgaaac
aggcacagccagaaccccaatcttcacaaaaacattccctttacttcaatagatggaagcggagctactaacttcagcctgctgaagcaggctggagacgtg
gaggagaaccctggacctatggtgcccaagaagaagaggaaagtctccaacctgctgactgtgcaccaaaacctgcctgccctccctgtggatgccacctc
tgatgaagtcaggaagaacctgatggacatgttcagggacaggcaggccttctctgaacacacctggaagatgctcctgtctgtgtgcagatcctgggctgcct
ggtgcaagctgaacaacaggaaatggttccctgctgaacctgaggatgtgagggactacctcctgtacctgcaagccagaggcctggctgtgaagaccatc
caacagcacctgggccagctcaacatgctgcacaggagatctggcctgcctcgcccttctgactccaatgctgtgtccctggtgatgaggagaatcagaaag
gagaatgtggatgctggggagagagccaagcaggccctggcctttgaacgcactgactttgaccaagtcagatccctgatggagaactctgacagatgcca
ggacatcaggaacctggccttcctgggcattgcctacaacacccctgctgcgcattgccgaaattgccagaatcagagtgaaggacatctcccgcaccgatgg
tgggagaatgctgatccacattggcaggaccaagaccctggtgtccacagctggtgtggagaaggccctgtccctgggggttaccaagctggtggagagat
ggatctctgtgtctggtgtggctgatgaccccaacaactacctgttctgccgggtcagaaagaatggtgtggctgccccttctgccacctcccaactgtccacccg
ggccctggaagggatctttgaggccacccaccgcctgatctatggtgccaaggatgactctgggcagagatacctggcctggtctggccactctgccagagtg
ggtgctgccagggacatggccagggctggtgtgtccatccctgaaatcatgcaggctggtggctggaccaatgtgaacattgtgatgaactacatcagaaac
ctggactctgagactggggccatggtgaggctgctcgaggatggggactgatcccagaacggacactccaaatgccagctctcaccagatggcctacatgtt
tgaactgccatagccagtgtgtgcttccgcagtggggcacatatgtgtgtacatatgtgtgcctctgtgtctacacttgtgcacacacatactttctttctttagata
aaaatgataaatactaggtgcttttgaaatttttttctttttcctttatagttttgggagagggtggatcttttacttggggtaaaaacaagagtgccctttcagcacaca
cacacacacacacacacacacacaaacacaacataacacacaaagtgtgcaactaaccccaattttgataggataattcttggtcttctccaaagagacattt
tgttgtacctatgactgttgcctgcaaaaacaataaataaataaaaggggaaaaaagagaaaagaaacaaaaaggaacttcttacagttgtct

Homology arm | P2A | NLS | iCre

c

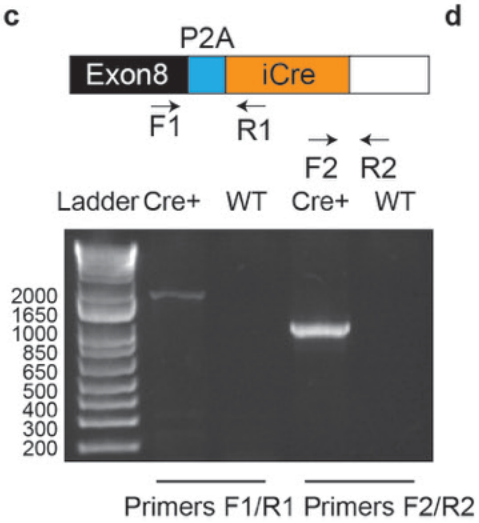

d

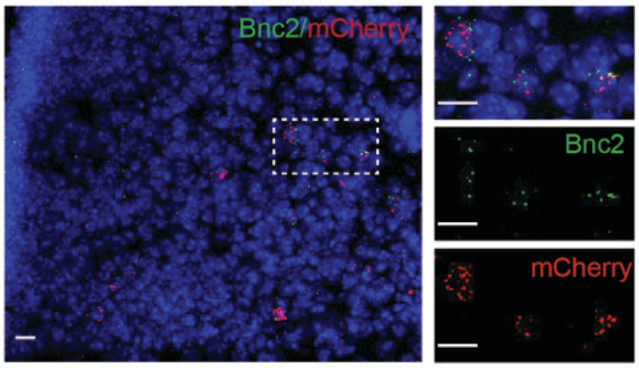

Extended Data Fig. 2: Generation of BNC2-P2A-iCre knockin mouse line. a, Schematic of BNC2-P2A-iCre locus. **b,** Sequence information of gRNAs and IssDNA. **c,** Genomic PCR using specific primers. **d,** Cre expression was marked using a Cre-dependent mCherry viral construct injection, and its colocalization with endogenous Bnc2 mRNA was confirmed through RNA ISH. Scale bar, 20 μm.

Extended Data Fig.3: Activation of BNC2 neurons by leptin

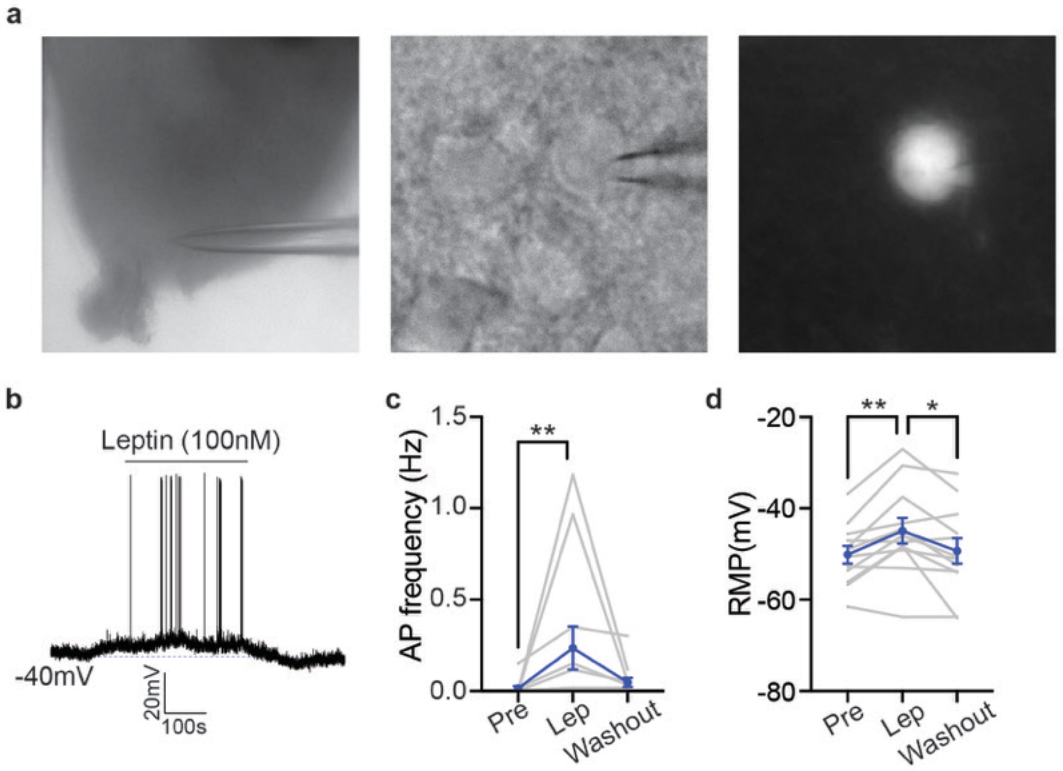

Extended Data Fig. 3: Activation of BNC2 neurons by leptin. a, Representative images of a patched GFP-labeled BNC2 neuron. **b,** Spontaneous APs of BNC2 neurons in ARC from ad-libitum-fed adult male BNC2-Cre mice (injected with DIO-GFP). Leptin (100 nM) was added to the bath solution at the indicated time window. **c,d,** Spontaneous AP frequency (**c**) and RMP (**d**) of BNC2 neurons before, during, and after leptin application (N = 12 cells from 4 mice). Data are presented as mean ± SEM. *$p<0.05$; **$p<0.01$. Details of the statistical analysis are provided as Source Data.

Extended Data Fig. 4: Rapid responses of BNC2 neurons to food cues.

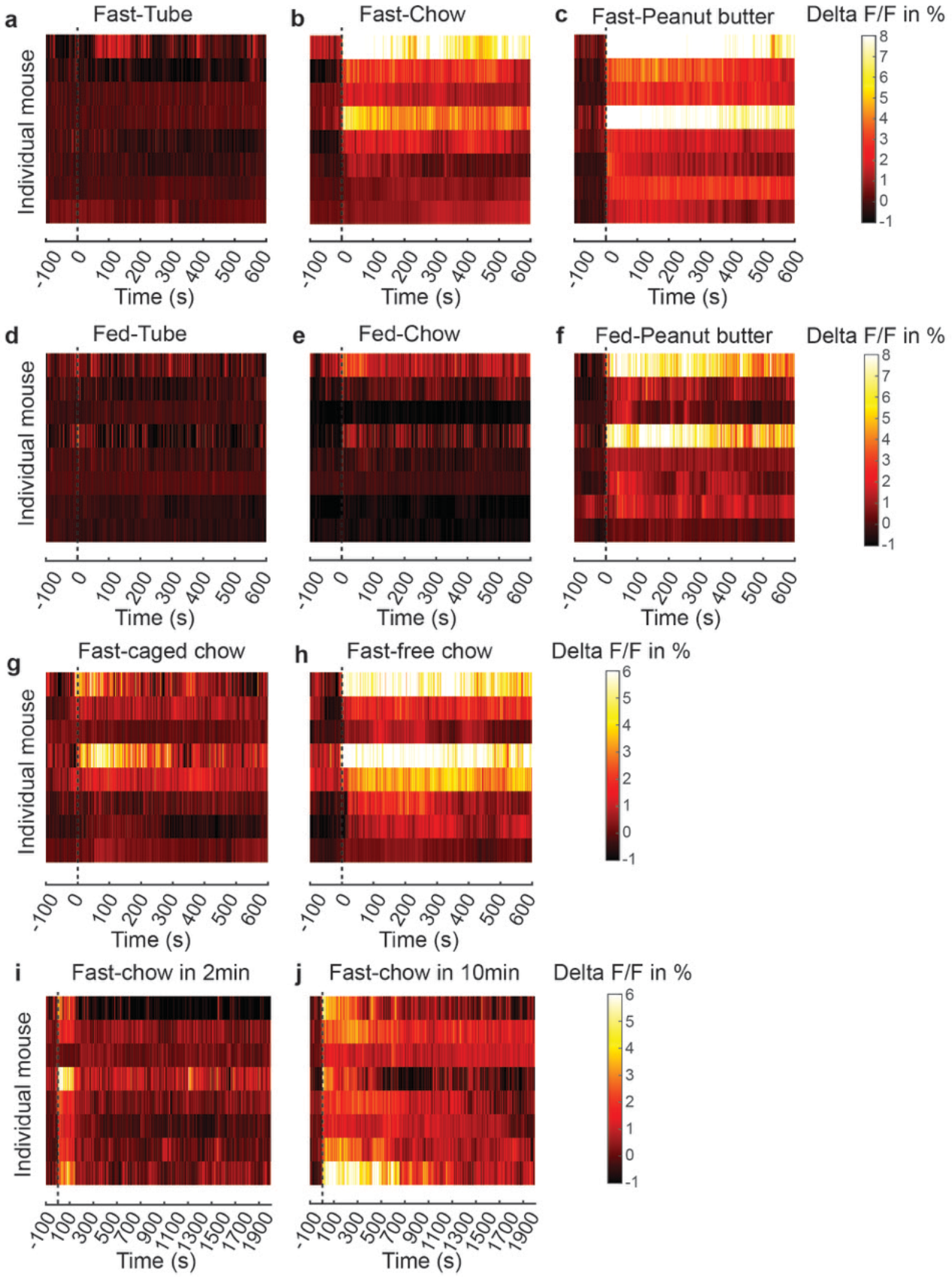

Extended Data Fig. 4: Rapid responses of BNC2 neurons to food cues. a-c, Heatmaps of normalized delta F/F in individual overnight fasted mice aligned to the time of the presentation of an inedible tube (**a**), chow (**b**), or peanut butter (**c**). **d-f,** Heatmaps of normalized delta F/F in individual ad-libitum-fed mice aligned to the time of the presentation of an inedible tube (**d**), chow (**e**), or peanut butter (**f**). **g,h,** Heatmaps of normalized delta F/F in individual overnight fasted mice aligned to the time of the presentation of a chow inside the container (**g**) and outside the container (**h**). **i,j,** Heatmaps of normalized delta F/F in individual overnight fasted mice aligned to the time of the presentation of chow for 2 minutes (**i**) and 10 minutes (**j**).

Extended Data Fig. 5: BNC2 neuron activation does not affect locomotion and place preference in sated mice

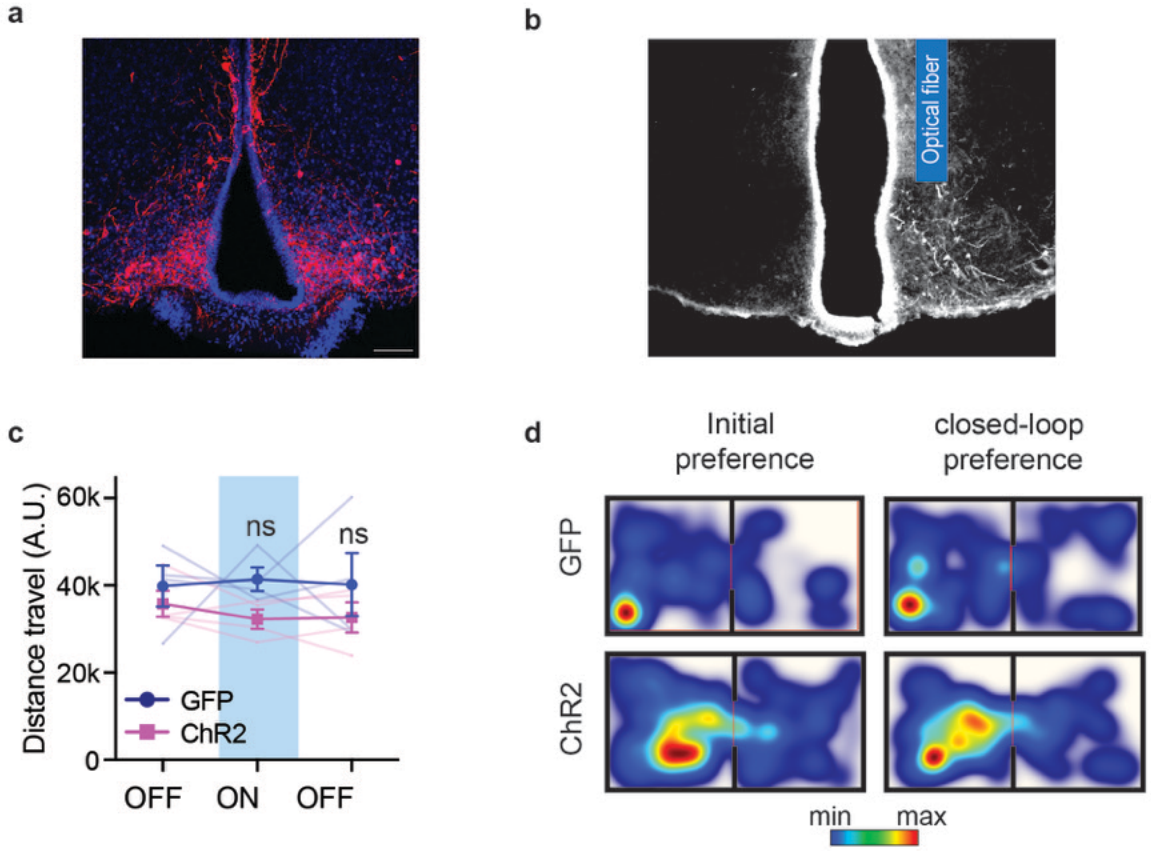

Extended Data Fig. 5: BNC2 neuron activation does not affect locomotion and place preference in sated mice. a, Representative image showing bilateral hM3Dq-mcherry expressing (red) in ARC BNC2 neurons. Blue, DAPI. Scale bar, 100 μm. **b,** Representative image showing unilateral ChR2-GFP expression in ARC BNC2 neurons and optical fiber implant site. **c,** Distance travel of mice before, during, and after the activation of laser stimulation in overnight-fasted mice (N = 4 mice per group). **d,** Heatmaps of time spent in each chamber of sated adult male BNC2-Cre mice injected with GFP or ChR2 during the initial phase and the closed-loop paired phase. Data are presented as mean ± SEM. ns, not significant. Details of the statistical analysis are provided as Source Data.

Extended Data Fig. 6: Light-induced activation of NPY neurons

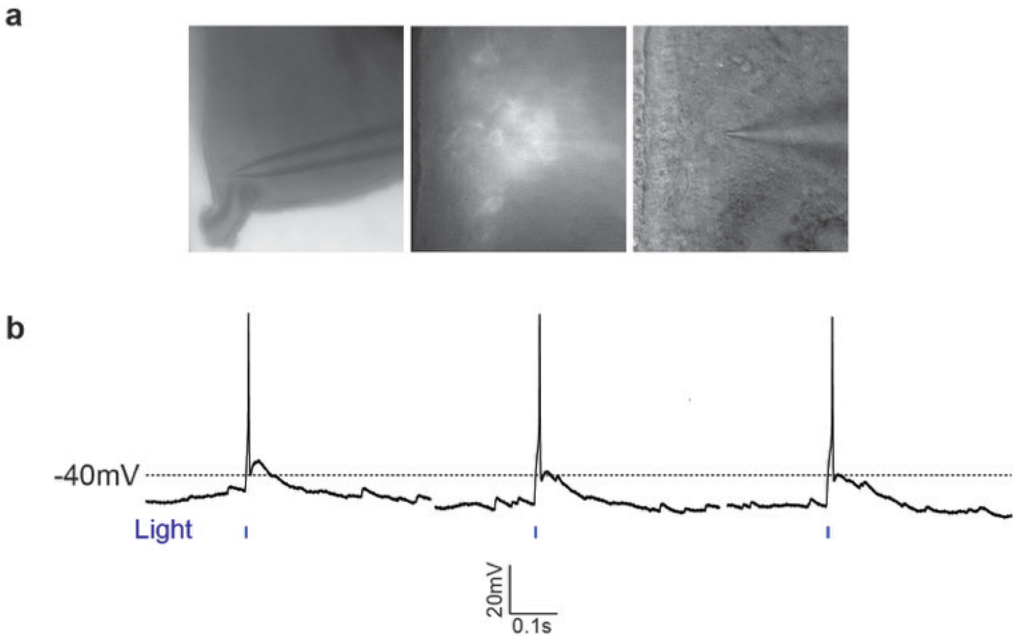

Extended Data Fig. 6: Light-induced activation of NPY neurons. a, Representative images of patched ChR2-GFP-labeled NPY neurons. **b,** Detection of light-induced APs in ChR2-GFP-labeled NPY neurons.

Extended Data Fig.7: High efficiency of Lepr deletion medated by sgLepr

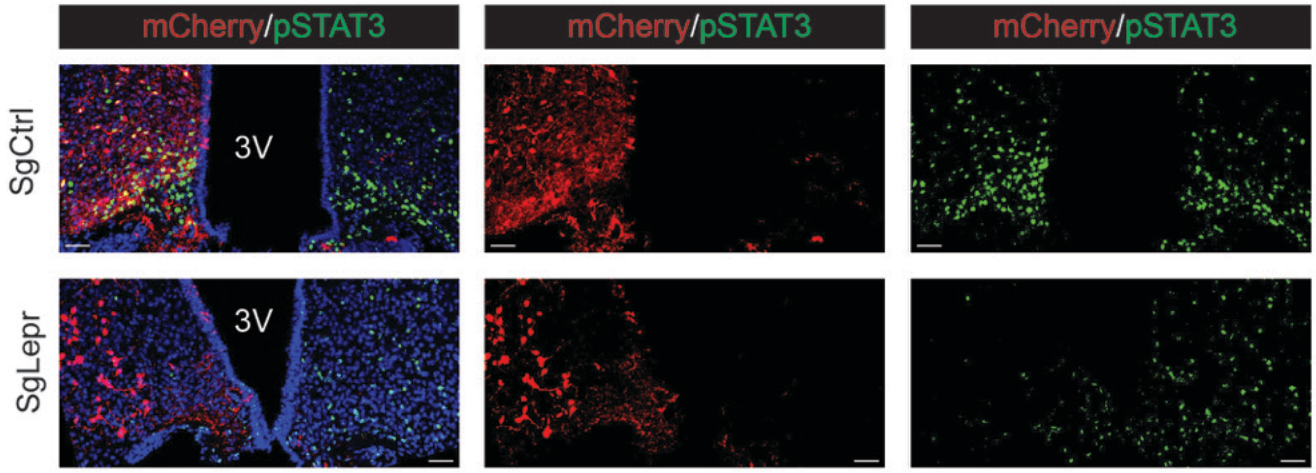

Extended Data Fig. 7: High efficiency of LepR deletion mediated by sgLepr. Brain slices from overnight fasted adult male BNC2-Cre::LSL-Cas9-GFP mice, injected with sgCtrl or sgLepr into the unilateral ARC, were subjected to mCherry and pSTAT3 immunostaining 3 hours after leptin injection. Scale bar, 50 μm.

Extended Data Fig.8: LepR knockout in BNC2 neurons causes higher RER

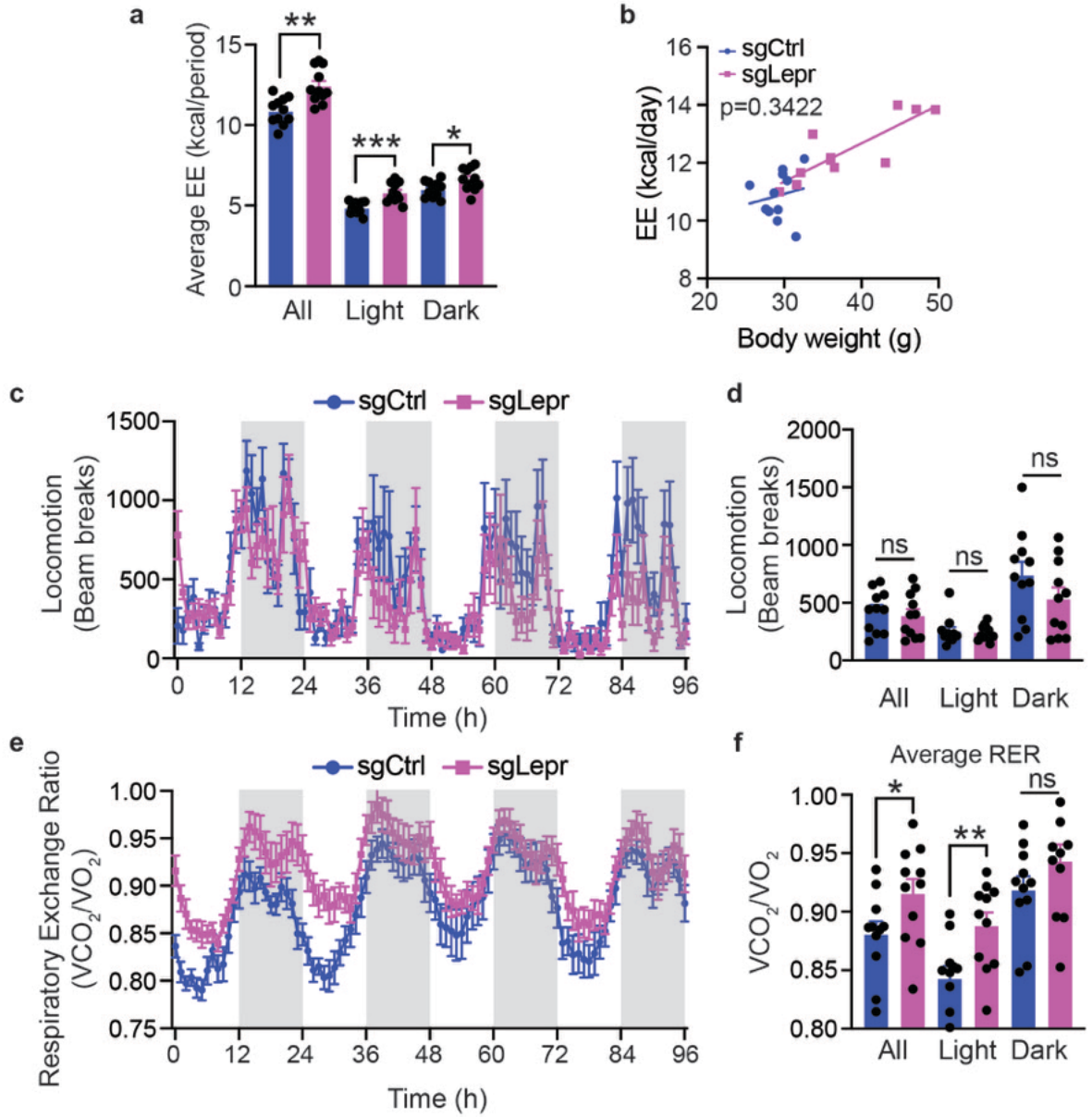

Extended Data Fig. 8: LepR knockout in BNC2 neurons causes higher RER. a, Quantification of EE of the two groups (N = 11 mice per group). **b,** Regression analysis of EE vs. total mass from **a** (N = 11 mice per group). **c,** Locomotion of the two groups of mice. **d,** Quantification of locomotion of the two groups (N = 11 mice per group). **e,** Respiratory exchange ratio (RER) of the two groups of mice. **f,** Quantification of average RER of two groups of mice (N = 11 mice per group). Data are presented as mean ± SEM. ns, not significant; *p<0.05. **p<0.01; ***p<0.001. Details of the statistical analysis are provided as Source Data.

Extended Data Fig.9: Model of leptin regulation of feeding and energy balance in ARC microcircuits

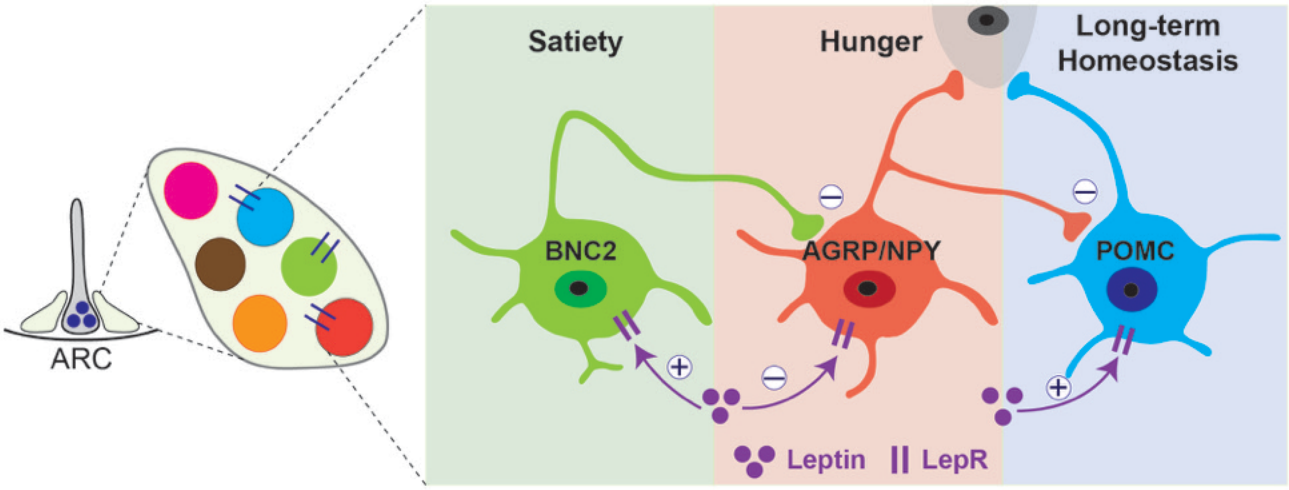

Extended Data Fig. 9: Model of leptin regulation of feeding and energy balance in ARC microcircuits. Leptin-activated BNC2 neurons acutely promote satiety by suppressing AGRP/NPY neurons, which rapidly stimulates hunger. POMC neurons restrict weight gain by modulating energy balance over the long term with minimal short-term effects on food intake.